NBS SPECIAL PUBLICATION 400-64

U.S. DEPARTMENT OF COMMERCE / National Bureau of Standards

Semiconductor Measurement Technology:

The Relationship Between Resistivity and Dopant Density for Phosphorus- and Boron-Doped Silicon

NATIONAL BUREAU OF STANDARDS

The National Bureau of Standards[1] was established by an act of Congress on March 3, 1901. The Bureau's overall goal is to strengthen and advance the Nation's science and technology and facilitate their effective application for public benefit. To this end, the Bureau conducts research and provides: (1) a basis for the Nation's physical measurement system, (2) scientific and technological services for industry and government, (3) a technical basis for equity in trade, and (4) technical services to promote public safety. The Bureau's technical work is performed by the National Measurement Laboratory, the National Engineering Laboratory, and the Institute for Computer Sciences and Technology.

THE NATIONAL MEASUREMENT LABORATORY provides the national system of physical and chemical and materials measurement; coordinates the system with measurement systems of other nations and furnishes essential services leading to accurate and uniform physical and chemical measurement throughout the Nation's scientific community, industry, and commerce; conducts materials research leading to improved methods of measurement, standards, and data on the properties of materials needed by industry, commerce, educational institutions, and Government; provides advisory and research services to other Government agencies; develops, produces, and distributes Standard Reference Materials; and provides calibration services. The Laboratory consists of the following centers:

Absolute Physical Quantities[2] — Radiation Research — Thermodynamics and Molecular Science — Analytical Chemistry — Materials Science.

THE NATIONAL ENGINEERING LABORATORY provides technology and technical services to the public and private sectors to address national needs and to solve national problems; conducts research in engineering and applied science in support of these efforts; builds and maintains competence in the necessary disciplines required to carry out this research and technical service; develops engineering data and measurement capabilities; provides engineering measurement traceability services; develops test methods and proposes engineering standards and code changes; develops and proposes new engineering practices; and develops and improves mechanisms to transfer results of its research to the ultimate user. The Laboratory consists of the following centers:

Applied Mathematics — Electronics and Electrical Engineering[2] — Mechanical Engineering and Process Technology[2] — Building Technology — Fire Research — Consumer Product Technology — Field Methods.

THE INSTITUTE FOR COMPUTER SCIENCES AND TECHNOLOGY conducts research and provides scientific and technical services to aid Federal agencies in the selection, acquisition, application, and use of computer technology to improve effectiveness and economy in Government operations in accordance with Public Law 89-306 (40 U.S.C. 759), relevant Executive Orders, and other directives; carries out this mission by managing the Federal Information Processing Standards Program, developing Federal ADP standards guidelines, and managing Federal participation in ADP voluntary standardization activities; provides scientific and technological advisory services and assistance to Federal agencies; and provides the technical foundation for computer-related policies of the Federal Government. The Institute consists of the following centers:

Programming Science and Technology — Computer Systems Engineering.

[1]Headquarters and Laboratories at Gaithersburg, MD, unless otherwise noted; mailing address Washington, DC 20234.
[2]Some divisions within the center are located at Boulder, CO 80303.

Semiconductor Measurement Technology:

The Relationship Between Resistivity and Dopant Density for Phosphorus- and Boron-Doped Silicon

W. R. Thurber, R.L. Mattis, and Y.M. Liu

Electron Devices Division
Center for Electronics and Electrical Engineering
National Engineering Laboratory
National Bureau of Standards
Washington, DC 20234

and

J. J. Filliben

Statistical Engineering Division
Center for Applied Mathematics
National Engineering Laboratory
National Bureau of Standards
Washington, DC 20234

This activity was supported by:

Defense Advanced Research Projects Agency
1400 Wilson Boulevard
Arlington, VA 22209

and

National Bureau of Standards
Washington, DC 20234

U.S. DEPARTMENT OF COMMERCE, Malcolm Baldrige, Secretary
NATIONAL BUREAU OF STANDARDS, Ernest Ambler, Director

Issued May 1981

Library of Congress Catalog Card Number: 81-600052

National Bureau of Standards Special Publication 400-64
Nat. Bur. Stand. (U.S.), Spec. Publ. 400-64, 53 pages (May 1981)
CODEN: XNBSAV

U.S. GOVERNMENT PRINTING OFFICE
WASHINGTON: 1981

For sale by the Superintendent of Documents, U.S. Government Printing Office, Washington, D.C. 20402
Price $3.25
(Add 25 percent for other than U.S. mailing)

TABLE OF CONTENTS

LIST OF FIGURES

LIST OF TABLES

Page

Semiconductor Measurement Technology:
The Relationship Between Resistivity and Dopant Density for Phosphorus- and Boron-Doped Silicon*

W. R. Thurber, R. L. Mattis, and Y. M. Liu†
Electron Devices Division
National Bureau of Standards
Washington, DC 20234

and

J. J. Filliben
Statistical Engineering Division
National Bureau of Standards
Washington, DC 20234

New data have been obtained for the resistivity-dopant density relationship for silicon doped with phosphorus or boron for dopant densities in the range 10^{13} to 10^{20} cm^{-3}. For dopant densities less than 10^{18} cm^{-3}, results were calculated from resistivity and junction capacitance-voltage measurements on processed wafers. For more heavily doped material, data were obtained from Hall effect and resistivity measurements on specimens cut from bulk silicon slices. These primary methods were supplemented for phosphorus-doped material by neutron activation analysis and a photometric technique and for boron-doped material by the nuclear track technique. For phosphorus-doped silicon the results of this work differ by 5 to 15 percent from the commonly used Irvin curve, always in the direction of lower resistivity for a given dopant density. For boron-doped silicon the results differ significantly from the *p*-type Irvin curve for boron densities greater than 10^{16} cm^{-3} with a maximum deviation of 45 percent at 5×10^{17} cm^{-3} in the direction of lower resistivity for a given dopant density. Hole mobility values derived from the data are in reasonable agreement with the Wagner expression with a maximum discrepancy of 10 percent in the 10^{18} cm^{-3} range. Analytical curves were fitted to the resistivity-dopant density product as a function of resistivity and dopant density for temperatures of both 23°C and 300 K. Similar curves were obtained for the calculated carrier mobility as a function of resistivity and carrier density.

Key Words: Boron; capacitance-voltage technique; dopant density; electron mobility; Hall effect; hole mobility; Irvin curves; phosphorus; resistivity; semiconductor; silicon.

---

* This work was conducted as part of the Semiconductor Technology Program at NBS and was supported in part by the Defense Advanced Research Projects Agency (Order No. 2397).

† Now with Westinghouse Advanced Technology Laboratory, Baltimore, MD 21203.

1. INTRODUCTION

The conversion between resistivity and dopant density of silicon is widely used in the semiconductor industry. In device design, the calculation of various parameters such as breakdown voltage involves relating resistivity, which can be readily measured, to dopant density, which is the desired quantity but very difficult to measure directly. Applications using the conversion over many decades of dopant density include the calculation of the surface dopant density of a diffused layer from the sheet resistance-junction depth product and the determination of a dopant density profile from incremental sheet resistance measurements. Significant error in the results of these measurements occurs when incorrect expressions are used to relate resistivity and dopant density.

During the past decade, the most frequently used conversion curves for both n- and p-type silicon are those formulated by Caughey and Thomas [1] based on the curves of Irvin [2]. Irvin's curve for n-type material includes measurements on silicon doped with arsenic, antimony, and phosphorus. More recently Baccarani and Ostoja [3] published a conversion for phosphorus-doped silicon which agrees with that of Irvin at low phosphorus densities but departs at high densities in the direction of lower resistivity for a given phosphorus density with a difference of 30 percent at 10^{20} cm^{-3}. Irvin's curve for p-type material includes measurements on silicon doped with aluminum, gallium, and boron. More recently Wagner [4] published a conversion for boron-doped silicon based on ion implantation results which differs from that of Irvin by up to 50 percent (in the direction of lower resistivity for a given boron density) for densities in the range 10^{16} to 10^{18} cm^{-3}. This report describes the results of a comprehensive redetermination of the resistivity-dopant density relationships for both phosphorus-doped silicon and boron-doped silicon and documents the results of the measurements upon which the redetermination was made. Papers have been published which summarize the results of this work on silicon doped with phosphorus [5] and with boron [6], but these papers do not contain either a complete record of the measurements used for the redetermination or a comprehensive discussion of many of the experimental and analytical details, both of which are included in this report.

2. MATERIAL SELECTION

The starting material, in both ingot and slice form, was obtained from several different suppliers and was selected for minimum resistivity gradients by mechanical four-probe array measurements [7] prior to use. For phosphorus-doped silicon, most of the results on high resistivity material were obtained on neutron transmutation doped silicon which proved much more uniform than material doped by more conventional techniques. The difference between center and half radius resistivity values ranged from -3 percent to +7 percent with an average absolute difference of +2.5 percent for the selected phosphorus-doped material and even less for the selected boron-doped material. Spreading resistance measurements were made on a number of ingots and slices to check on fine structure in the resistivity. All of the boron-doped material was very uniform, but a slight fine structure with a period of about 1 mm and a peak-to-valley variation of about 15 percent was seen in some of the phosphorus-doped material.

3. TEST STRUCTURE MEASUREMENTS

For dopant densities of 10^{18} cm^{-3} or less, resistivity and dopant density data were obtained from microelectronic test structures fabricated on silicon slices. The resistivity was measured directly on planar four-probe square array structures described in detail elsewhere [8]. A cross-sectional view of this structure is shown in figure 1. The dopant density was determined from capacitance-voltage (C-V) measurements [9] on gated p-n junction diodes. These test structures and other diagnostic structures were assembled on microelectronic test patterns NBS-3 [10] and NBS-4 [11] which were prepared especially for this work.

The patterns were fabricated on the silicon slices by bipolar processing [12]. Various measurements were made on the wafers to verify the fabrication and to assure that leakage currents were low enough for proper operation of the test structures. The resistivity data obtained from the square array structures agreed to within a few percent with mechanical four-probe measurements [13] made prior to fabrication.

The dopant density was measured by the C-V method [9] on the gated base-collector diode structure shown schematically in figure 2. This method gives the net dopant density, i.e., the number of dopant atoms in excess of any compensating atoms on the more lightly doped side of the junction. For meaningful C-V measurements, it is important to bias the gate at the flat-band voltage which was determined from C_{min} - C_{max} measurements on an MOS capacitor structure of the test pattern [14]. The dopant density calculated from the C-V method is particularly sensitive to the value used for the diameter of the diode as the diameter enters as the fourth power. The diameter (nominally 432 μm) of several diodes was measured by the NBS line-standard scanning interferometer [15]. These results were then used as a calibration for determining from photomicrographs the diameters of other diodes from each processing run of wafers. The uncertainty in the measured diameter is estimated to be less than 1 μm. The base junction depth, used in the analysis of the C-V data, was measured by the groove and stain technique [16] with an estimated error of $\pm$0.1 μm.

Dopant density values were calculated from the C-V data using a computer program which includes corrections for peripheral effects and takes into account the fraction of the total depletion depth which occurs in the diffused layer [17]. A fitting procedure [18] was incorporated into the program in which a Gaussian shape is assumed for the base diffusion near the junction, and the surface concentration of the diffusion and the background dopant density are adjusted to give a best fit to all the C-V data. The fitting procedure made it possible to obtain results on wafers with dopant densities up to 7 x 10^{17} cm^{-3}; otherwise, wafers with dopant density greater than 10^{17} cm^{-3} could not be measured because of compensation by the diffusion tail within the depletion depth obtainable in the substrate before voltage breakdown occurs. This fitting procedure was used for reducing the C-V data to dopant density for all wafers except a few of the lightly doped ones. For these lightly doped wafers, the program was used without the iterative fitting procedure as the diffused layer effects are negligible. Some lightly doped wafers were analyzed both ways, and the dopant density values were the same with the

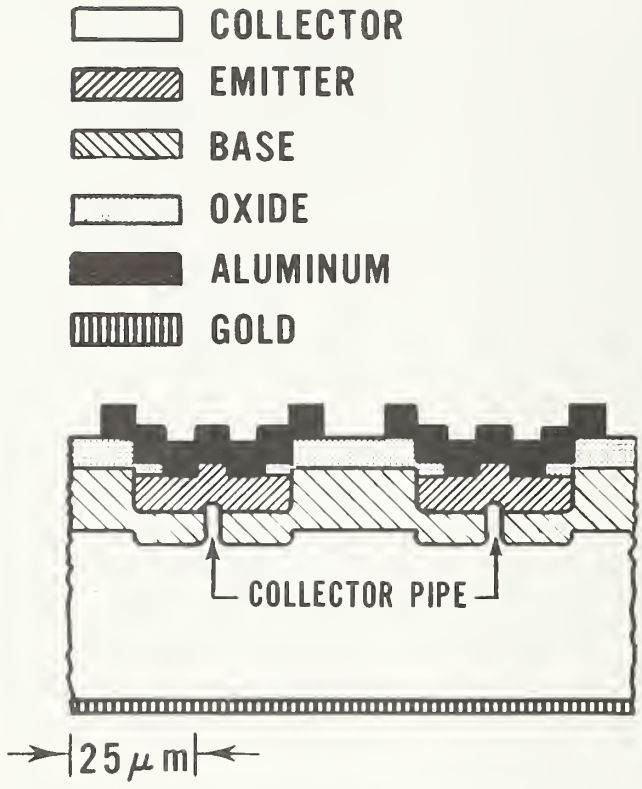

Figure 1. Schematic cross-sectional view of the four-probe resistor test structure. The pipes are arranged in a square configuration with a center-to-center spacing of 57.2 μm (2.25 mil).

fitting procedure as without. In the calculations, a value of 11.7 [19] was used for the relative dielectric constant of silicon.

The square array resistivity results were corrected to both 23°C and 300 K from the actual measurement temperatures using published coefficients for the change of resistivity with temperature [20]. The measurement temperature was determined by a copper-constantan thermocouple imbedded in the vacuum chuck holding the wafer on a probe station. The C-V measurements were made at room temperature with no correction for temperature as the dopant is completely ionized in the depletion layer.

The procedure used for correlating the resistivity and dopant density values was slightly different for the two test patterns. The one four-probe resistor structure contained on test pattern NBS-3 is not located in the same cell as the diode used for the dopant density measurements. In order to minimize the influence of resistivity variations over the wafer, the average of the resistivities measured on the two four-probe resistors on either side of the diode was taken as the resistivity corresponding to the dopant density at that diode site. On test pattern NBS-4, there are four four-probe resistor structures with different collector pipe sizes for measuring a wide range of resistivities in the cell containing the base-collector diode. On this pattern, an average resistivity was obtained from measurements on two or more adjacent four-probe structures in the cell containing the diode. Differences between minimum and maximum values of resistivity in a given cell rarely exceeded 1 percent for boron-doped material but were in the range from 1 to 5 percent for phosphorus-doped material because of the localized resistivity variations characteristic of most phosphorus-doped silicon. Typically, for wafers fabricated with either test pattern, data were collected for six cells near the center of each wafer and the results averaged. Mobility values calculated for a few of the wafers were judged significantly below those from other wafers with similar dopant densities. The wafers with low mobility were omitted from the results so that the curves would represent good material without appreciable compensation or other problems.

The estimated error in the planar four-probe resistivity measurements is about 1 percent. Factors which contribute to the error are finite wafer thickness, pipe spacing uncertainty, instrument calibration, and temperature measurement. Errors in the dopant density due to uncertainties in the surface dopant density of the diffusion, junction depth, and random measurement error were examined in idealized data studies [18]. The errors caused by uncertainties in these parameters for the wafers in this work were shown to be less than one percent. Additional error in the dopant density arises from uncertainties in diode diameter, flat-band voltage, and instrument calibration, giving a total estimated error of 2 percent. Resistivity gradients in the wafers are an additional source of error in that the resistivity at the diode site may be different from that measured at the four-probe sites as discussed above. Consequently, for phosphorus-doped material, even after averaging over six sites, the total error may be as large as 5 percent. For the more uniform boron-doped material, the total error is in the range of 3 percent.

Figure 2. Cross-sectional view of the base-collector diode used for the junction C-V measurements of dopant density.

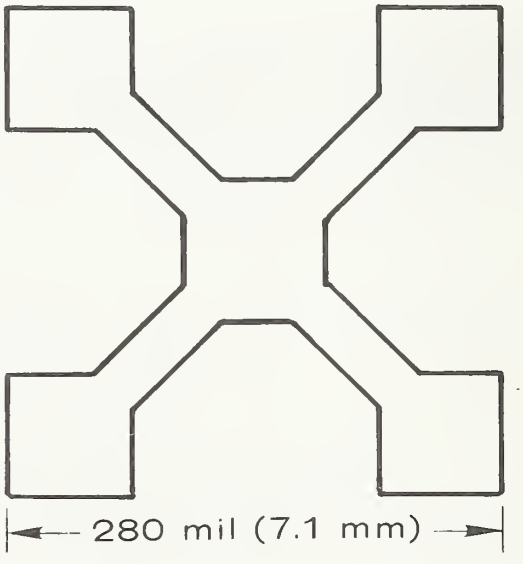

Figure 3. Shape of van der Pauw specimens ultrasonically cut from bulk silicon slices.

4. HALL EFFECT MEASUREMENTS

For dopant densities greater than 10^{19} cm^{-3}, Hall effect and resistivity measurements were made on van der Pauw specimens [21] ultrasonically cut from bulk silicon slices. The shape of the specimens is shown in figure 3. For selected slices, a Greek cross design [22] was also cut. The measurements were made at controlled temperatures of both 23°C and 300 K for a magnetic flux density of 0.6 T (6 kG) following standard procedures [23]. The commercial Hall probe for measuring the flux density was calibrated using an NMR gaussmeter. The integrating digital voltmeter used for all the voltage measurements was calibrated using a standard voltage source and a standard cell calibrated at NBS. The standard resistors used for the determination of the current through the specimens were calibrated against other standard resistors with known values. Resistivity values obtained from the van der Pauw specimens were within a few percent of the four-probe values measured on the respective wafers during the material selection process.

For phosphorus-doped silicon the electron density, n, was calculated from the expression $n = -r/qR_H$, where q is the electronic charge, R_H is the Hall coefficient, and r is the Hall scattering factor [24]. For heavily doped n-type material, r is unity.

For boron-doped silicon the hole density, p, was calculated from the expression $p = r/qR_H$. Due to the complex nature of the valence band of silicon, the factor r for p-type material is less than unity, even for heavily doped specimens. In this work r was taken equal to 0.8 as the majority of experimental results [25-28] and recent calculations [29] on moderately doped material suggest a value in this range. No measurements of r for dopant densities greater than 2×10^{18} cm^{-3} appear to be available for p-type silicon.

Results obtained on the van der Pauw specimens have an estimated error of less than 3 percent for phosphorus-doped material. Most of this error is in the Hall coefficient as it is more difficult to measure accurately than is the resistivity. The measurement-related error is the same for boron-doped material, but the uncertainty in r contributes an additional, unknown error. There is the probability that r differs from 0.8 by ± 0.1. This corresponds to an error of up to 15 percent in p.

5. RESULTS FOR PHOSPHORUS-DOPED SILICON

Table 1 gives the data for phosphorus-doped silicon obtained from measurements on test patterns. Under wafer identification in column 1 are listed: (1) the wafer number, (2) the initial resistivity at 23°C from four-probe array measurements at the center of the wafer before processing, (3) the test pattern used for fabrication, and (4) the measured diameter, D, in micrometers of the diodes used for the C-V measurements of dopant density, N, in column 3. The site listed in column 2 gives the x-y coordinates of the diode on the wafer. The diode in the approximate center of the wafer is designated 0,0 and the others are referenced with respect to it. For example -1,1 specifies the diode located one unit (200 mils) in the -x direction and one unit in the +y direction from the reference diode. Columns 4 and 5 give the resistivity values measured using the four-probe resistor structures and corrected to 23°C and 300 K, respectively. Column 6 gives the electron density

Table 1. Data for Phosphorus-Doped Silicon Obtained from Test Patterns.

Wafer Identification	Site	N cm^{-3}	$\rho_{23°C}$ Ω·cm	$\rho_{300\ K}$ Ω·cm	n cm^{-3}	$\mu_{23°C}$ $cm^2/V·s$	$\mu_{300\ K}$ $cm^2/V·s$
G140Ph-1	0,0	2.699×10^{13}	158.3	163.3	2.699×10^{13}	1461	1413
ρ_i = 137	-1,0	2.691×10^{13}	158.8	163.9	2.691×10^{13}	1461	1415
NBS-4	-1,1	2.598×10^{13}	159.0	164.1	2.598×10^{13}	1511	1464
D = 433.3	0,1	2.671×10^{13}	158.7	163.8	2.671×10^{13}	1472	1427
	1,1	2.790×10^{13}	158.4	163.4	2.790×10^{13}	1412	1369
	1,0	2.757×10^{13}	158.1	163.2	2.757×10^{13}	1432	1387
	Avg.	2.701×10^{13}	158.6	163.6	2.701×10^{13}	1458 ± 34	1413 ± 33
C100Ph-1	1,0	3.893×10^{13}	110.3	113.8	3.893×10^{13}	1454	1409
ρ_i = 98	0,0	3.854×10^{13}	107.0	110.4	3.854×10^{13}	1514	1467
NBS-4	-1,0	3.933×10^{13}	111.2	114.8	3.933×10^{13}	1427	1382
D = 433.3	-1,1	3.555×10^{13}	116.1	119.8	3.555×10^{13}	1512	1466
	0,1	3.963×10^{13}	114.4	118.0	3.963×10^{13}	1377	1335
	1,1	4.015×10^{13}	109.7	113.2	4.015×10^{13}	1417	1373
	Avg.	3.869×10^{13}	111.4	115.0	3.869×10^{13}	1450 ± 55	1405 ± 53
G65Ph-1	0,0	6.201×10^{13}	68.07	70.25	6.201×10^{13}	1479	1433
ρ_i = 67.4	-1,0	6.147×10^{13}	69.50	71.72	6.147×10^{13}	1461	1416
NBS-4	-1,1	5.892×10^{13}	69.70	71.93	5.892×10^{13}	1520	1473
D = 433.3	0,1	6.141×10^{13}	69.92	72.15	6.141×10^{13}	1454	1409
	1,1	6.358×10^{13}	69.26	71.47	6.358×10^{13}	1417	1374
	1,0	6.127×10^{13}	69.70	71.93	6.127×10^{13}	1462	1416
	2,0	6.007×10^{13}	69.60	71.82	6.007×10^{13}	1493	1447
	Avg.	6.125×10^{13}	69.39	71.61	6.125×10^{13}	1469 ± 32	1424 ± 31
C30Ph-1	1,0	1.149×10^{14}	37.42	38.62	1.149×10^{14}	1452	1407
ρ_i = 31.9	0,0	1.150×10^{14}	37.29	38.48	1.150×10^{14}	1455	1410
NBS-4	-1,0	1.114×10^{14}	37.30	38.49	1.114×10^{14}	1502	1456
D = 433.3	-1,1	1.126×10^{14}	37.33	38.52	1.126×10^{14}	1485	1439
	0,1	1.155×10^{14}	37.35	38.54	1.155×10^{14}	1447	1402
	1,1	1.153×10^{14}	37.46	38.66	1.153×10^{14}	1445	1400
	Avg.	1.141×10^{14}	37.36	38.55	1.141×10^{14}	1464 ± 23	1419 ± 23
B12Ph-1	-1,0	3.557×10^{14}	13.15	13.57	3.557×10^{14}	1334	1293
ρ_i = 11.8	-1,1	3.248×10^{14}	12.65	13.06	3.248×10^{14}	1519	1471
NBS-3	0,1	3.623×10^{14}	12.82	13.23	3.623×10^{14}	1344	1302
D = 433.8	1,1	3.174×10^{14}	13.29	13.72	3.174×10^{14}	1480	1433
	-1,2	3.253×10^{14}	13.34	13.77	3.253×10^{14}	1438	1393
	0,2	3.363×10^{14}	13.37	13.80	3.363×10^{14}	1388	1345
	1,2	3.102×10^{14}	12.91	13.33	3.102×10^{14}	1559	1509
	-2,1	3.429×10^{14}	12.62	13.03	3.429×10^{14}	1442	1397
	-2,-1	3.206×10^{14}	13.24	13.67	3.206×10^{14}	1470	1424
	1,-1	3.241×10^{14}	12.87	13.29	3.241×10^{14}	1496	1449
	Avg.	3.320×10^{14}	13.03	13.45	3.320×10^{14}	1447 ± 74	1402 ± 71
D9.5Ph-1	1,0	4.025×10^{14}	10.01	10.34	4.025×10^{14}	1549	1500
ρ_i = 9.51	0,0	4.552×10^{14}	10.03	10.36	4.552×10^{14}	1367	1324
NBS-3	0,1	4.234×10^{14}	10.58	10.92	4.234×10^{14}	1393	1350
D = 433.1	-1,1	4.540×10^{14}	10.23	10.56	4.540×10^{14}	1344	1302
	-1,0	4.297×10^{14}	9.94	10.26	4.297×10^{14}	1461	1416
	-1,-1	4.339×10^{14}	10.04	10.37	4.339×10^{14}	1433	1387
	Avg.	4.331×10^{14}	10.14	10.47	4.331×10^{14}	1425 ± 74	1380 ± 72

Table 1 - Continued

Wafer Identification	Site	N cm^{-3}	$\rho_{23°C}$ Ω·cm	$\rho_{300\ K}$ Ω·cm	n cm^{-3}	$\mu_{23°C}$ $cm^2/V·s$	$\mu_{300\ K}$ $cm^2/V·s$
F9.1Ph-1	0,0	4.814×10^{14}	9.107	9.391	4.814×10^{14}	1424	1381
ρ_i = 9.1	-1,0	4.745×10^{14}	9.203	9.490	4.745×10^{14}	1429	1386
NBS-4	0,1	4.723×10^{14}	9.283	9.572	4.723×10^{14}	1424	1381
D = 433.3	1,1	4.732×10^{14}	9.208	9.496	4.732×10^{14}	1432	1389
	1,0	4.800×10^{14}	9.225	9.513	4.800×10^{14}	1410	1367
	-2,1	4.802×10^{14}	9.079	9.363	4.802×10^{14}	1432	1388
	Avg.	4.769×10^{14}	9.184	9.471	4.769×10^{14}	1425 ± 8	1382 ± 8
B5.9Ph-1	0,0	7.646×10^{14}	5.699	5.875	7.646×10^{14}	1432	1389
ρ_i = 5.94	-1,0	7.158×10^{14}	6.481	6.681	7.158×10^{14}	1345	1305
NBS-4	-1,1	7.363×10^{14}	6.116	6.304	7.363×10^{14}	1386	1345
D = 433.3	0,1	7.272×10^{14}	5.940	6.123	7.272×10^{14}	1445	1402
	1,1	7.167×10^{14}	6.327	6.522	7.167×10^{14}	1376	1335
	1,0	6.297×10^{14}	6.468	6.667	6.297×10^{14}	1532	1487
	Avg.	7.150×10^{14}	6.172	6.362	7.150×10^{14}	1419 ± 66	1377 ± 65
D2.4Ph-1	-1,1	1.946×10^{15}	2.353	2.426	1.946×10^{15}	1363	1322
ρ_i = 2.35	0,1	1.968×10^{15}	2.275	2.346	1.968×10^{15}	1394	1352
NBS-3	1,1	2.058×10^{15}	2.352	2.425	2.058×10^{15}	1289	1250
D = 433.1	-1,0	1.966×10^{15}	2.372	2.446	1.966×10^{15}	1338	1298
	0,0	1.842×10^{15}	2.429	2.504	1.842×10^{15}	1395	1354
	1,0	1.941×10^{15}	2.405	2.480	1.941×10^{15}	1337	1297
	-1,-1	1.878×10^{15}	2.432	2.508	1.878×10^{15}	1367	1325
	0,-1	1.874×10^{15}	2.455	2.531	1.874×10^{15}	1357	1316
	Avg.	1.934×10^{15}	2.384	2.458	1.934×10^{15}	1355 ± 34	1314 ± 33
B2.1Ph-2	0,0	2.185×10^{15}	2.129	2.192	2.185×10^{15}	1342	1303
ρ_i = 2.14	1,0	2.321×10^{15}	1.994	2.053	2.321×10^{15}	1349	1310
NBS-4	1,1	2.368×10^{15}	1.976	2.035	2.368×10^{15}	1334	1295
D = 433.3	0,1	2.281×10^{15}	2.003	2.062	2.281×10^{15}	1366	1327
	-1,1	2.438×10^{15}	1.950	2.008	2.438×10^{15}	1313	1275
	-1,0	2.389×10^{15}	1.978	2.037	2.389×10^{15}	1321	1283
	Avg.	2.330×10^{15}	2.005	2.064	2.330×10^{15}	1338 ± 19	1299 ± 19
B1.4Ph-3	-1,1	3.749×10^{15}	1.358	1.398	3.749×10^{15}	1226	1191
ρ_i = 1.29	0,1	3.707×10^{15}	1.314	1.353	3.707×10^{15}	1281	1244
NBS-3	1,1	3.404×10^{15}	1.301	1.340	3.404×10^{15}	1409	1368
D = 433.1	-1,0	3.460×10^{15}	1.297	1.335	3.460×10^{15}	1391	1351
	0,0	3.859×10^{15}	1.253	1.290	3.859×10^{15}	1291	1254
	1,0	3.278×10^{15}	1.296	1.334	3.278×10^{15}	1469	1427
	0,-1	3.553×10^{15}	1.392	1.433	3.553×10^{15}	1262	1226
	Avg.	3.573×10^{15}	1.316	1.355	3.573×10^{15}	1332 ± 90	1295 ± 87
A1.0Ph-1	0,-1	4.800×10^{15}	1.019	1.049	4.800×10^{15}	1276	1240
ρ_i = 1.01	-1,0	4.885×10^{15}	1.005	1.034	4.885×10^{15}	1271	1236
NBS-3	-1,1	4.596×10^{15}	1.024	1.054	4.596×10^{15}	1326	1288
D = 432.8	-2,1	4.675×10^{15}	1.040	1.071	4.675×10^{15}	1284	1247
	Avg.	4.739×10^{15}	1.022	1.052	4.739×10^{15}	1289 ± 25	1253 ± 24
B0.80Ph-1	1,0	6.098×10^{15}	0.7887	0.8106	6.098×10^{15}	1298	1263
ρ_i = 0.79	0,0	6.716×10^{15}	0.7643	0.7855	6.716×10^{15}	1216	1183
NBS-4	1,1	6.353×10^{15}	0.7834	0.8051	6.353×10^{15}	1254	1220
D = 433.3	0,1	5.920×10^{15}	0.8122	0.8347	5.920×10^{15}	1298	1263
	-1,1	5.958×10^{15}	0.8067	0.8291	5.958×10^{15}	1299	1264
	-1,0	6.211×10^{15}	0.7807	0.8023	6.211×10^{15}	1287	1253
	Avg.	6.210×10^{15}	0.7893	0.8112	6.210×10^{15}	1275 ± 34	1241 ± 33

Table 1 - Continued

Wafer Identification	Site	N cm^{-3}	$\rho_{23°C}$ $\Omega \cdot cm$	$\rho_{300\ K}$ $\Omega \cdot cm$	n cm^{-3}	$\mu_{23°C}$ $cm^2/V \cdot s$	$\mu_{300\ K}$ $cm^2/V \cdot s$
B0.77Ph-1	0,1	6.251×10^{15}	0.7912	0.8138	6.251×10^{15}	1262	1227
ρ_i = 0.77	1,1	6.400×10^{15}	0.7771	0.7993	6.400×10^{15}	1255	1220
NBS-3	-1,0	6.630×10^{15}	0.7656	0.7874	6.630×10^{15}	1230	1196
D = 433.1	0,0	6.673×10^{15}	0.7647	0.7865	6.673×10^{15}	1223	1189
	1,0	6.257×10^{15}	0.7731	0.7951	6.257×10^{15}	1290	1255
	0,-1	5.955×10^{15}	0.7990	0.8218	5.955×10^{15}	1312	1275
	Avg.	6.361×10^{15}	0.7785	0.8007	6.361×10^{15}	1262 ± 34	1227 ± 33
B0.47Ph-1	0,0	1.132×10^{16}	0.4834	0.4964	1.131×10^{16}	1142	1112
ρ_i = 0.47	0,1	1.175×10^{16}	0.4856	0.4987	1.174×10^{16}	1095	1066
NBS-3	-1,0	1.122×10^{16}	0.4778	0.4907	1.121×10^{16}	1165	1135
D = 432.8	-1,1	1.072×10^{16}	0.4912	0.5044	1.071×10^{16}	1186	1155
	-2,1	0.974×10^{16}	0.5027	0.5162	0.973×10^{16}	1276	1243
	-2,0	1.027×10^{16}	0.5133	0.5271	1.026×10^{16}	1185	1154
	-1,-1	1.115×10^{16}	0.4735	0.4862	1.114×10^{16}	1183	1152
	1,0	1.032×10^{16}	0.4965	0.5099	1.031×10^{16}	1219	1187
	Avg.	1.081×10^{16}	0.4905	0.5037	1.080×10^{16}	1181 ± 53	1150 ± 52
B0.40Ph-1	-1,-1	1.485×10^{16}	0.3586	0.3677	1.484×10^{16}	1173	1144
ρ_i = 0.40	0,0	1.145×10^{16}	0.4442	0.4555	1.144×10^{16}	1228	1198
NBS-4	-1,0	1.303×10^{16}	0.4201	0.4308	1.302×10^{16}	1141	1270
D = 433.3	-1,1	1.226×10^{16}	0.4545	0.4660	1.225×10^{16}	1121	1093
	0,1	1.186×10^{16}	0.4542	0.4657	1.185×10^{16}	1160	1131
	1,1	1.807×10^{16}	0.3280	0.3363	1.806×10^{16}	1054	1028
	1,0	1.603×10^{16}	0.3605	0.3697	1.602×10^{16}	1081	1054
	0,-1	1.198×10^{16}	0.4115	0.4220	1.197×10^{16}	1267	1236
	1,-1	1.624×10^{16}	0.3532	0.3622	1.623×10^{16}	1089	1062
	Avg.	1.397×10^{16}	0.3983	0.4084	1.396×10^{16}	1146 ± 70	1101 ± 75
B0.30Ph-1	0,0	2.004×10^{16}	0.2845	0.2915	2.000×10^{16}	1097	1071
ρ_i = 0.285	1,0	1.945×10^{16}	0.2869	0.2940	1.941×10^{16}	1121	1094
NBS-4	1,1	2.110×10^{16}	0.2782	0.2851	2.106×10^{16}	1065	1040
D = 433.3	0,1	2.025×10^{16}	0.2899	0.2970	2.021×10^{16}	1065	1040
	-1,1	2.070×10^{16}	0.2828	0.2898	2.066×10^{16}	1068	1042
	-1,0	2.046×10^{16}	0.2872	0.2943	2.042×10^{16}	1064	1039
	Avg.	2.033×10^{16}	0.2849	0.2920	2.029×10^{16}	1080 ± 24	1054 ± 23
A0.27Ph-2	0,0	2.171×10^{16}	0.2748	0.2815	2.165×10^{16}	1049	1024
ρ_i = 0.269	0,1	2.093×10^{16}	0.2708	0.2774	2.087×10^{16}	1104	1078
NBS-3	-1,0	2.094×10^{16}	0.2673	0.2738	2.088×10^{16}	1118	1092
D = 432.8	-1,1	2.090×10^{16}	0.2746	0.2813	2.084×10^{16}	1091	1065
	Avg.	2.112×10^{16}	0.2719	0.2785	2.106×10^{16}	1090 ± 30	1065 ± 29
B0.18Ph-2	0,0	3.308×10^{16}	0.1900	0.1943	3.288×10^{16}	999	977
ρ_i = 0.192	-1,0	3.342×10^{16}	0.1927	0.1970	3.322×10^{16}	975	954
NBS-4	-1,1	3.267×10^{16}	0.1924	0.1967	3.247×10^{16}	999	977
D = 433.3	0,1	3.177×10^{16}	0.1980	0.2024	3.158×10^{16}	998	976
	1,1	3.356×10^{16}	0.1911	0.1953	3.336×10^{16}	979	958
	1,0	3.235×10^{16}	0.1953	0.1997	3.215×10^{16}	994	972
	Avg.	3.281×10^{16}	0.1932	0.1976	3.261×10^{16}	991 ± 11	969 ± 10
B0.12Ph-1	-1,0	5.730×10^{16}	0.1225	0.1250	5.667×10^{16}	899	881
ρ_i = 0.124	0,0	5.514×10^{16}	0.1221	0.1245	5.453×10^{16}	937	919
NBS-4	1,0	6.691×10^{16}	0.1249	0.1274	6.617×10^{16}	755	740
D = 433.3	-1,1	5.667×10^{16}	0.1070	0.1091	5.604×10^{16}	1041	1021
	0,1	5.840×10^{16}	0.1289	0.1315	5.776×10^{16}	838	822
	1,1	5.041×10^{16}	0.1235	0.1260	4.985×10^{16}	1014	994
	-1,-1	5.981×10^{16}	0.1152	0.1175	5.915×10^{16}	916	898
	1,-1	5.932×10^{16}	0.1296	0.1322	5.867×10^{16}	821	805
	Avg.	5.800×10^{16}	0.1217	0.1242	5.736×10^{16}	903 ± 97	885 ± 95

Table 1 - Continued

Wafer Identification	Site	N cm^{-3}	$\rho_{23°C}$ Ω·cm	$\rho_{300\ K}$ Ω·cm	n cm^{-3}	$\mu_{23°C}$ $cm^2/V \cdot s$	$\mu_{300\ K}$ $cm^2/V \cdot s$
B0.099Ph-3	-1,1	8.965×10^{16}	0.09077	0.09238	8.831×10^{16}	779	765
ρ_i = 0.092	-1,0	9.557×10^{16}	0.08933	0.09091	9.414×10^{16}	742	729
NBS-4	0,0	9.735×10^{16}	0.08695	0.08849	9.589×10^{16}	749	735
D = 433.3	1,0	8.766×10^{16}	0.08959	0.09118	8.635×10^{16}	807	793
	1,1	9.555×10^{16}	0.09381	0.09547	9.412×10^{16}	707	695
	0,1	9.078×10^{16}	0.08953	0.09112	8.942×10^{16}	780	766
	Avg.	9.276×10^{16}	0.09000	0.09159	9.137×10^{16}	761 ± 35	747 ± 34
B0.080Ph-1	1,-1	1.131×10^{17}	0.07776	0.07905	1.109×10^{17}	724	712
ρ_i = 0.080	-1,-1	1.090×10^{17}	0.07835	0.07965	1.069×10^{17}	745	733
NBS-4	-1,1	1.101×10^{17}	0.07943	0.08074	1.080×10^{17}	728	716
D = 433.3	0,1	1.053×10^{17}	0.08100	0.08234	1.033×10^{17}	746	734
	1,1	1.165×10^{17}	0.07881	0.08011	1.143×10^{17}	693	682
	1,0	1.086×10^{17}	0.08004	0.08137	1.065×10^{17}	732	720
	0,0	1.039×10^{17}	0.08058	0.08191	1.019×10^{17}	760	748
	0,-1	1.090×10^{17}	0.07891	0.08022	1.069×10^{17}	740	728
	Avg.	1.094×10^{17}	0.07936	0.08067	1.073×10^{17}	734 ± 20	722 ± 20
A0.060Ph-3	-1,0	1.459×10^{17}	0.06375	0.06466	1.421×10^{17}	689	679
ρ_i = 0.062	-1,1	1.544×10^{17}	0.06473	0.06565	1.504×10^{17}	641	632
NBS-4	0,1	1.808×10^{17}	0.05920	0.06004	1.761×10^{17}	599	590
D = 433.3	1,1	1.576×10^{17}	0.06189	0.06277	1.535×10^{17}	657	648
	1,0	1.566×10^{17}	0.06042	0.06128	1.525×10^{17}	677	668
	0,0	1.913×10^{17}	0.05820	0.05903	1.863×10^{17}	576	568
	Avg.	1.644×10^{17}	0.06137	0.06224	1.601×10^{17}	640 ± 44	631 ± 44
B0.050Ph-3	1,2	2.234×10^{17}	0.05285	0.05350	2.160×10^{17}	547	540
ρ_i = 0.051	0,2	2.145×10^{17}	0.05115	0.05178	2.074×10^{17}	588	581
NBS-4	1,3	2.135×10^{17}	0.05439	0.05506	2.064×10^{17}	556	549
D = 433.3	0,3	2.114×10^{17}	0.05334	0.05400	2.044×10^{17}	572	566
	-1,3	2.070×10^{17}	0.05453	0.05520	2.001×10^{17}	572	565
	Avg.	2.140×10^{17}	0.05325	0.05391	2.069×10^{17}	567 ± 16	560 ± 16
B0.034Ph-1	-1,0	5.112×10^{17}	0.03410	0.03438	4.811×10^{17}	380	377
ρ_i = 0.034	-1,1	4.764×10^{17}	0.03481	0.03509	4.483×10^{17}	400	397
NBS-4	0,1	4.284×10^{17}	0.03527	0.03556	4.031×10^{17}	439	435
D = 433.3	1,1	4.782×10^{17}	0.03422	0.03450	4.500×10^{17}	405	402
	1,0	5.081×10^{17}	0.03434	0.03462	4.781×10^{17}	380	377
	0,0	5.386×10^{17}	0.03508	0.03536	5.068×10^{17}	351	348
	Avg.	4.901×10^{17}	0.03464	0.03492	4.612×10^{17}	392 ± 30	389 ± 29
B0.031Ph-1	-1,1	5.085×10^{17}	0.03152	0.03172	4.775×10^{17}	415	412
ρ_i = 0.032	0,1	5.067×10^{17}	0.03200	0.03220	4.758×10^{17}	410	407
NBS-4	1,1	5.290×10^{17}	0.03149	0.03169	4.967×10^{17}	399	396
D = 433.1	-1,0	5.437×10^{17}	0.03157	0.03177	5.105×10^{17}	387	385
	0,0	5.740×10^{17}	0.02991	0.03010	5.390×10^{17}	387	385
	1,0	4.827×10^{17}	0.03297	0.03318	4.532×10^{17}	418	415
	Avg.	5.241×10^{17}	0.03158	0.03178	4.921×10^{17}	403 ± 14	400 ± 13

calculated from the dopant density using the results of Li and Thurber [30] for the fraction of dopant which is ionized. Columns 7 and 8 give the electron mobility, μ, calculated for temperatures of both 23°C and 300 K, respectively, using the relationship $\mu = 1/qn\rho$ where q is the electronic charge, n is the electron density, and ρ is the resistivity.

Table 2 gives the Hall coefficient, electron density, resistivity, and mobility for the phosphorus-doped silicon van der Pauw specimens measured at both 23°C and 300 K. A comparison of the Hall coefficient results at the two temperatures gives a measure of the experimental reproducibility as the Hall coefficient at 23°C should be essentially the same as that at 300 K. The results are usually within 0.2 percent, and the largest discrepancy is 0.5 percent. In all cases the resistivity at 300 K is larger than at 23°C as expected from the positive temperature coefficient of resistivity [20].

In addition to the C-V and Hall effect work discussed in this report, neutron activation analysis and photometric measurements of total phosphorus density were made outside NBS on material used in this study. These techniques and a comparison of the results obtained from them are discussed in detail elsewhere [31]. A complete listing of data for slices analyzed by neutron activation analysis is given in table 3. Data for slices analyzed by the photometric technique are given in table 4.

Figure 4 shows the product of resistivity and dopant density as a function of resistivity at 300 K. Since, to a first approximation, resistivity is inversely proportional to dopant density, a plot of the product allows deviations from this inverse relationship to be more easily seen, particularly for low resistivities where the product is large. As seen in figure 4, there is a systematic difference between the results from neutron activation analysis and those from the photometric technique. The data points from the Hall effect, which measures only electrically active phosphorus, lie between the two nonelectrical techniques. Neutron activation analysis and C-V agree within experimental error for phosphorus densities in the range of 10^{16} to 5×10^{17} cm^{-3}. The data of Mousty *et al.* [32], obtained from resistivity measurements and either neutron activation analysis or Hall effect for phosphorus density, are also plotted in figure 4. Their results are in reasonable agreement with this work except at the low resistivity end where differences are as large as 15 percent.

Throughout the resistivity range, the data obtained in the present study are displaced from the Irvin curve [2], also shown in figure 4, in the direction of lower dopant density for a given resistivity. The difference varies between 5 and 15 percent over the resistivity range with somewhat larger deviations below 1 $\Omega \cdot cm$ than above.

Figure 5 is a graph of electron mobility at 300 K as a function of electron density. The theoretical curve of Li and Thurber [30] is in good agreement with the experimental results. The Caughey and Thomas [1] mobility expression for *n*-type silicon gives significantly lower mobility at low electron density. The Caughey and Thomas expression is a fit to the Irvin curve with the assumption that the electron density equals the dopant density. This is true for lightly doped material ($<10^{17}$ cm^{-3}), but calculations [30] indicate that the electron density is less than the dopant density for material in the

Table 2. Data for Phosphorus-Doped Silicon Obtained from van der Pauw Specimens.

Specimen No.	T = 23°C				T = 300 K			
	$R_H(cm^3/C)$	$n(cm^{-3})$	$\rho(\Omega \cdot cm)$	$\mu(cm^2/V \cdot s)$	$R_H(cm^3/C)$	$n(cm^{-3})$	$\rho(\Omega \cdot cm)$	$\mu(cm^2/V \cdot s)$
0.0047Ph-A	-0.4815	1.296×10^{19}	0.004766	101.0	-0.4812	1.297×10^{19}	0.004781	100.6
0.0045Ph-39	-0.4365	1.430×10^{19}	0.004335	100.7	-0.4367	1.429×10^{19}	0.004353	100.3
0.0033Ph-L31	-0.3167	1.971×10^{19}	0.003304	95.8	-0.3172	1.968×10^{19}	0.003322	95.5
0.0026Ph-A	-0.2150	2.903×10^{19}	0.002327	92.4	-0.2146	2.908×10^{19}	0.002345	91.5
0.0020Ph-47	-0.1802	3.464×10^{19}	0.002000	90.1	-0.1792	3.483×10^{19}	0.002015	88.9
0.0020Ph-19	-0.1783	3.501×10^{19}	0.001984	89.9	-0.1780	3.506×10^{19}	0.001999	89.1
0.0017Ph-A	-0.1431	4.362×10^{19}	0.001597	89.6	-0.1430	4.365×10^{19}	0.001611	88.8
0.0015Ph-A	-0.1286	4.853×10^{19}	0.001444	89.1	-0.1289	4.842×10^{19}	0.001456	88.5
0.0012Ph-A	-0.1068	5.844×10^{19}	0.001225	87.2	-0.1065	5.860×10^{19}	0.001235	86.2
0.0013Ph-46	-0.1047	5.961×10^{19}	0.001200	87.3	-0.1046	5.967×10^{19}	0.001210	86.4
0.0011Ph-A	-0.0879	7.101×10^{19}	0.001044	84.2	-0.0881	7.084×10^{19}	0.001054	83.6
0.0009Ph-A	-0.0690	9.046×10^{19}	0.000857	80.5	-0.0693	9.006×10^{19}	0.000864	80.2

Table 3. Data for Silicon Slices with the Phosphorus Density Determined by Neutron Activation Analysis.

Slice No.	$\rho_{23°C}$ Ω·cm	N cm^{-3}
46-1	0.00129	$5.85 \pm 0.11 \times 10^{19}$
47-1	0.00201	$3.66 \pm 0.10 \times 10^{19}$
39-1	0.00448	$1.54 \pm 0.01 \times 10^{19}$
26-1	0.00697	$9.10 \pm 0.09 \times 10^{18}$
52-1	0.0101	$5.25 \pm 0.10 \times 10^{18}$
52-3	0.0105	$4.93 \pm 0.08 \times 10^{18}$
25-1	0.0340	$4.51 \pm 0.10 \times 10^{17}$
48-1	0.0520	$2.28 \pm 0.08 \times 10^{17}$
48-2	0.0531	$2.12 \pm 0.05 \times 10^{17}$
34-1	0.0785	$1.20 \pm 0.01 \times 10^{17}$
34-2	0.0759	$1.19 \pm 0.04 \times 10^{17}$
51-1	0.193	$3.9 \pm 0.6 \times 10^{16}$
40-1	0.281	$2.03 \pm 0.13 \times 10^{16}$
70-1	0.404	$1.50 \pm 0.05 \times 10^{16}$
70-2	0.387	$1.53 \pm 0.07 \times 10^{16}$
29-1	0.492	$1.16 \pm 0.08 \times 10^{16}$
38-1	0.805	$7.35 \pm 0.35 \times 10^{15}$
49-2	1.40	$4.99 \pm 0.39 \times 10^{15}$

Table 4. Data for Silicon Slices with the Phosphorus Density Determined by the Photometric Technique.

Slice No.	$\rho_{23°C}$ Ω·cm	N cm^{-3}
46-2	0.00130	5.17×10^{19}
47-2	0.00219	3.02×10^{19}
L31-5	0.00378	1.65×10^{19}
39-2	0.00457	1.22×10^{19}
26-2	0.00730	7.70×10^{18}
52-2	0.0101	4.44×10^{18}
14-A	0.0144	2.40×10^{18}
25-L	0.0333	4.30×10^{17}
48-L	0.0501	2.27×10^{17}

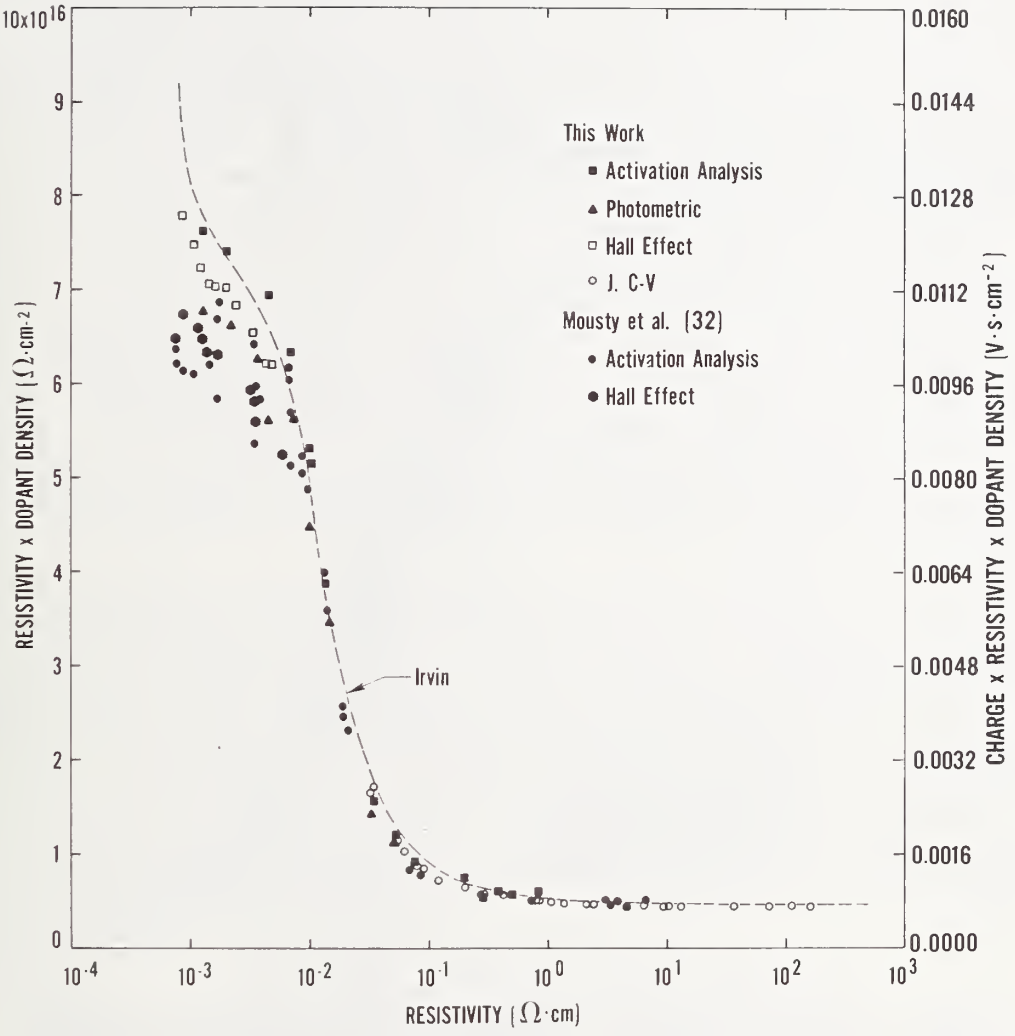

Figure 4. Resistivity-dopant density product for phosphorus-doped silicon at 300 K. Results of this work are compared with those of Mousty *et al.* [32] and Irvin [2]. Values of the qρN product are on the right ordinate.

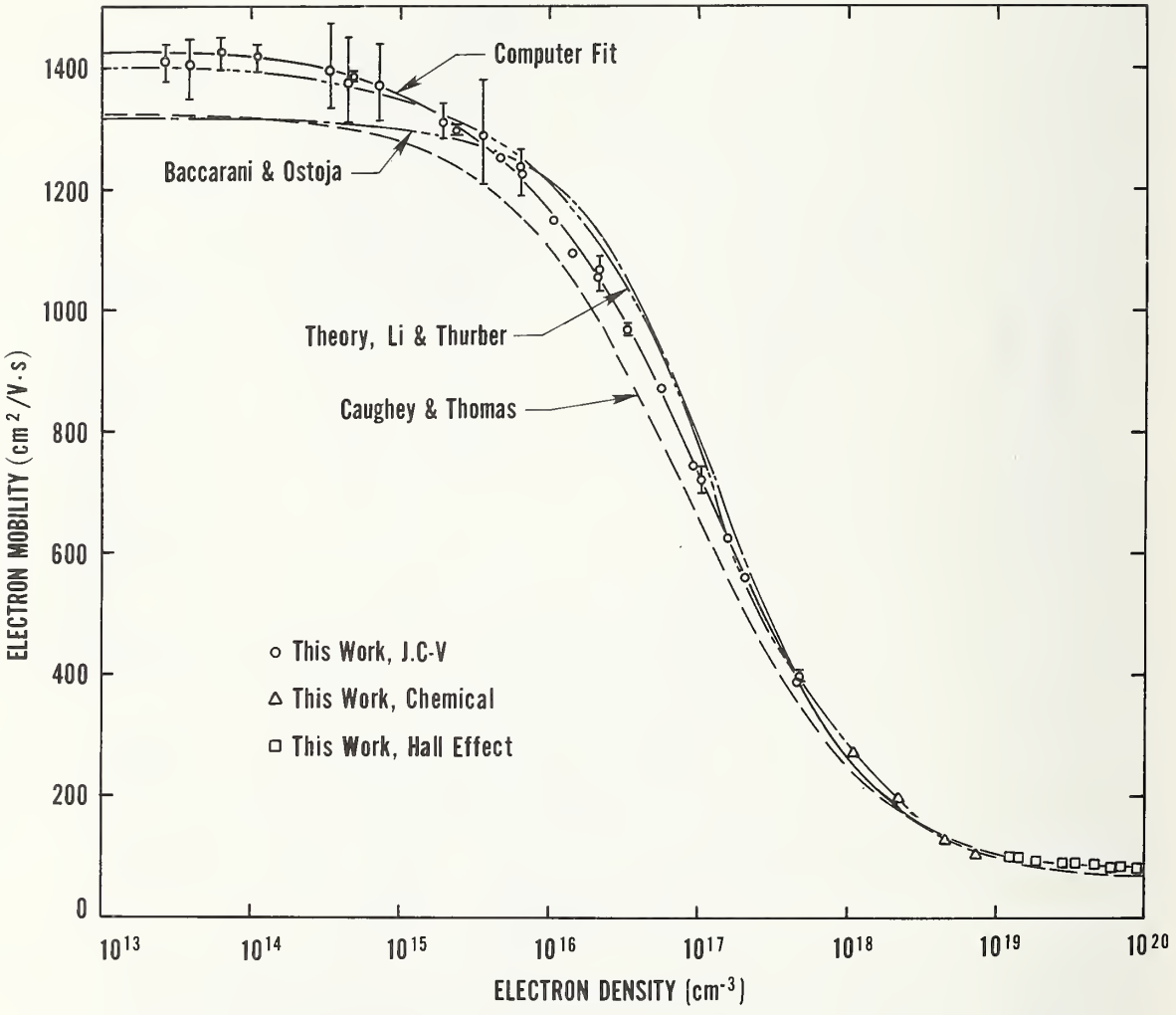

Figure 5. Electron mobility as a function of electron density for phosphorus-doped silicon at 300 K. The junction C-V data have been corrected for deionization using the calculations of Li and Thurber [30]. The error bars are the standard deviation in the individual mobility values for that wafer. When not shown, the error bars lie within the plotted symbol. Shown for comparison with the computer fit to the data are the mobility expressions of Caughey and Thomas [1], Baccarani and Ostoja [3], and the theoretical calculation of Li and Thurber [30].

10^{17} cm^{-3} to mid-10^{18} cm^{-3} range. In the heavily doped range, the two densities are again equal except for the formation of phosphorus-vacancy pairs, which give rise to electrically inactive atoms, at phosphorus densities greater than about 5 x 10^{19} cm^{-3} [33].

Also shown in figure 5 is the mobility expression of Baccarani and Ostoja [3] based on the data of Mousty *et al.* [32], with the assumption that electron and dopant densities are equal. For comparison with the other curves the Baccarani and Ostoja expression has been corrected to 300 K since the Mousty data were taken at 23°C. At low dopant densities, the Baccarani and Ostoja curve is about 7 percent below the data of this work. In the range 10^{16} to 5 x 10^{17} cm^{-3}, their curve is parallel to, but about 5 percent above, the results of this work. At high dopant densities, the Baccarani and Ostoja curve gives values between 10 and 20 percent larger than those obtained in this work as is seen more clearly in figure 6, which is a detailed expansion of the high density portion of figure 5.

In figure 6, all of the results shown were obtained by Hall effect and resistivity measurements with the assumption that the Hall scattering factor was unity. In this dopant range, the Caughey and Thomas curve is lower and the Baccarani and Ostoja curve is higher than the results of this work. The modification of the Caughey-Thomas expression shown in the figure consists of multiplying the constant μ_{min} in the Caughey-Thomas expression by a term which decreases μ_{min} at high electron densities [34]. The computer fit to the present data (open rectangular points) is also shown in figure 6.

With the exception of the data point of Fair and Tsai [35], all of the results in figure 6 were obtained on silicon doped during crystal growth. Recently, Masetti and Solmi [36] have made extensive measurements on silicon heavily doped by thermal diffusion. Their mobility values obtained from incremental sheet resistance and Hall effect measurements are in good agreement with those of this work. They concluded, from a comparison of their data with those of Mousty *et al.*, that the mobility in diffused phosphorus-doped silicon is always lower than that in uniformly doped silicon for $n > 10^{19}$ cm^{-3}. However, when the results of Masetti and Solmi are compared with those of this work, the conclusion is that the mobility is the same in diffused and uniformly doped silicon.

6. RESULTS FOR BORON-DOPED SILICON

Table 5 gives the data for boron-doped silicon derived from measurements on test patterns. The items listed and the symbols used are the same as those for table 1 except for the hole density, p, which was obtained from the dopant density using the ionization percentages calculated by Li [37]. Table 6 gives data on boron-doped silicon slices obtained by the nuclear track technique (NTT) [38]. Table 7 lists the results obtained from Hall effect measurements at both 23°C and 300 K. For calculating the hole density, the scattering factor was taken equal to 0.8 as discussed in section 4. This value was also used to obtain hole density from the Hall measurements of Chapman *et al.* [39] and Crowder [40].

Figure 7 is a graph of the product of resistivity and dopant density as a function of resistivity at 300 K. The NTT results are seen to be in good

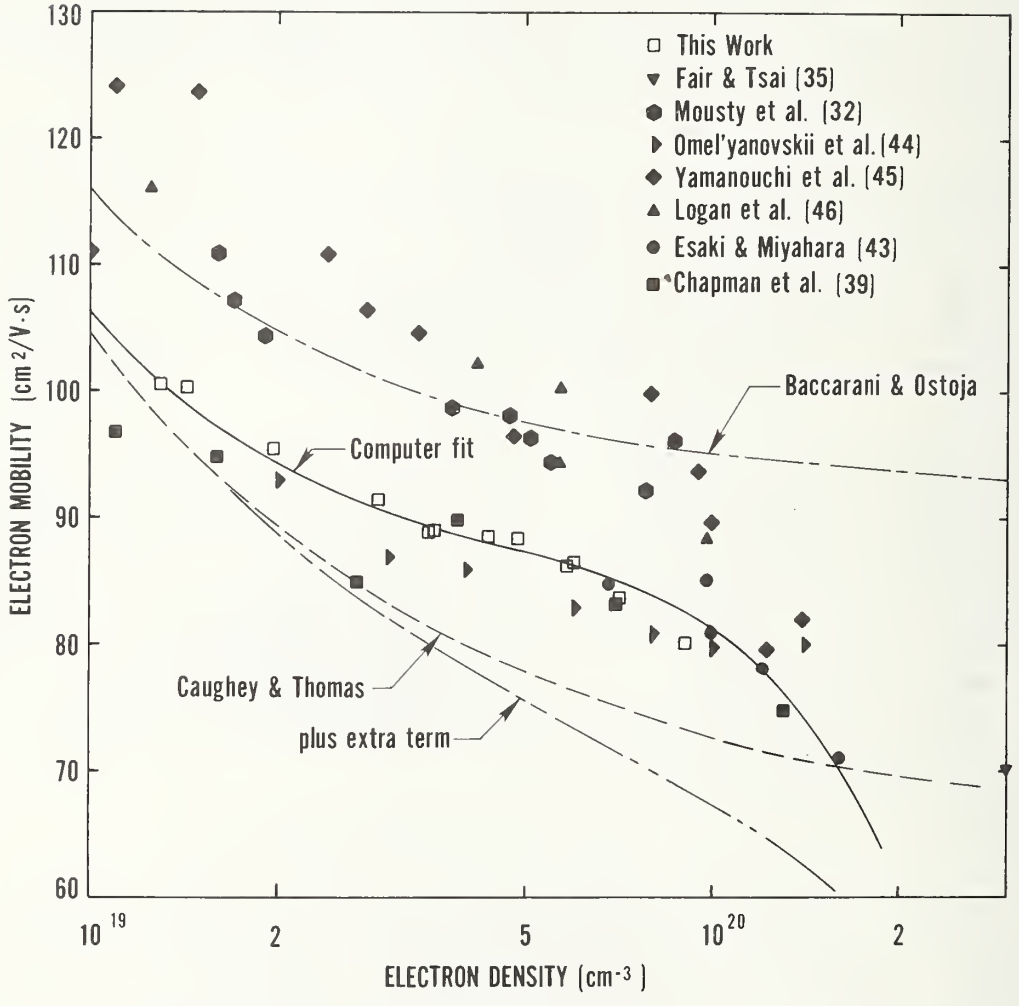

Figure 6. Electron mobility determined from Hall effect measurements for electron densities greater than 10^{19} cm^{-3}. The computer fit to the data of this work lies between the mobility expressions of Caughey and Thomas [1] and Baccarani and Ostoja [3]. The extra term in the modified Caughey and Thomas expression is given by Plunkett *et al.* [34].

Table 5. Data for Boron-Doped Silicon Obtained from Test Patterns.

Wafer Identification	Site	N cm^{-3}	$\rho_{23°C}$ Ω·cm	$\rho_{300\ K}$ Ω·cm	p cm^{-3}	$\mu_{23°C}$ $cm^2/V·s$	$\mu_{300\ K}$ $cm^2/V·s$
B94B-3	-1,1	1.284×10^{14}	94.68	97.85	1.284×10^{14}	513.4	496.8
ρ_i = 94.0	0,1	1.362×10^{14}	97.50	100.77	1.362×10^{14}	470.0	454.8
NBS-4	1,1	1.266×10^{14}	96.48	99.71	1.266×10^{14}	511.0	494.4
D = 432.8	-1,0	1.362×10^{14}	98.00	101.28	1.362×10^{14}	467.6	452.5
	0,0	1.373×10^{14}	99.62	102.96	1.373×10^{14}	456.3	441.5
	1,0	1.313×10^{14}	94.80	97.98	1.313×10^{14}	501.4	485.2
	1,-1	1.328×10^{14}	97.66	100.93	1.328×10^{14}	481.2	465.7
	0,-1	1.310×10^{14}	96.35	99.28	1.310×10^{14}	494.5	479.9
	Avg.	1.325×10^{14}	96.89	100.10	1.325×10^{14}	486.9 ± 21.3	471.4 ± 20.7
B49B-3	-1,1	2.547×10^{14}	50.99	52.68	2.547×10^{14}	480.6	465.2
ρ_i = 48.8	0,1	2.537×10^{14}	49.42	51.06	2.537×10^{14}	497.8	481.8
NBS-4	1,1	2.640×10^{14}	49.26	50.89	2.640×10^{14}	479.9	464.6
D = 432.8	-1,0	2.625×10^{14}	49.30	50.93	2.625×10^{14}	482.3	466.9
	0,0	2.648×10^{14}	49.50	51.14	2.648×10^{14}	476.2	460.9
	1,0	2.608×10^{14}	49.66	51.30	2.608×10^{14}	481.9	466.5
	Avg.	2.601×10^{14}	49.69	51.33	2.601×10^{14}	483.1 ± 7.5	467.6 ± 7.3
C21B-2	-1,1	6.258×10^{14}	20.79	21.48	6.258×10^{14}	479.7	464.3
ρ_i = 22.0	0,1	6.267×10^{14}	20.81	21.50	6.267×10^{14}	478.6	463.2
NBS-4	1,1	6.454×10^{14}	20.57	21.25	6.454×10^{14}	470.1	455.1
D = 433.3	-1,0	6.248×10^{14}	20.80	21.49	6.248×10^{14}	488.1	464.8
	0,0	6.203×10^{14}	20.82	21.51	6.203×10^{14}	483.3	467.8
	1,0	6.219×10^{14}	20.54	21.22	6.219×10^{14}	488.6	473.0
	Avg.	6.275×10^{14}	20.72	21.41	6.275×10^{14}	481.4 ± 6.9	464.7 ± 5.9
B9.0B-3	0,0	1.489×10^{15}	8.971	9.254	1.489×10^{15}	467.2	453.0
ρ_i = 9.0	1,0	1.453×10^{15}	8.911	9.192	1.453×10^{15}	482.0	467.3
NBS-4	1,1	1.488×10^{15}	8.997	9.281	1.488×10^{15}	466.2	451.9
D = 433.3	-1,0	1.478×10^{15}	8.948	9.230	1.478×10^{15}	471.9	457.5
	-2,0	1.479×10^{15}	8.848	9.127	1.479×10^{15}	476.9	462.4
	-1,2	1.489×10^{15}	8.900	9.181	1.489×10^{15}	471.0	456.6
	0,2	1.487×10^{15}	8.994	9.278	1.487×10^{15}	466.7	452.4
	1,2	1.455×10^{15}	8.966	9.249	1.455×10^{15}	478.4	463.8
	Avg.	1.477×10^{15}	8.942	9.224	1.477×10^{15}	472.5 ± 6.0	458.1 ± 5.8
B5.7B-4	-1,1	2.307×10^{15}	5.753	5.932	2.300×10^{15}	471.7	457.5
ρ_i = 5.7	0,1	2.294×10^{15}	5.795	5.976	2.287×10^{15}	470.9	456.7
NBS-4	1,1	2.333×10^{15}	5.767	5.947	2.326×10^{15}	465.3	451.2
D = 433.8	-1,0	2.312×10^{15}	5.742	5.921	2.305×10^{15}	471.6	457.3
	0,0	2.353×10^{15}	5.648	5.824	2.346×10^{15}	471.0	456.8
	1,0	2.342×10^{15}	5.731	5.910	2.335×10^{15}	466.4	452.3
	Avg.	2.324×10^{15}	5.739	5.918	2.317×10^{15}	469.5 ± 2.9	455.3 ± 2.8
B3.0B-3	-1,1	4.756×10^{15}	2.946	3.037	4.733×10^{15}	447.6	434.2
ρ_i = 3.0	0,1	4.731×10^{15}	2.949	3.040	4.708×10^{15}	449.5	436.1
NBS-4	-1,0	4.643×10^{15}	2.974	3.066	4.620×10^{15}	454.3	440.6
D = 433.3	0,0	4.689×10^{15}	2.967	3.059	4.666×10^{15}	450.8	437.3
	1,0	4.673×10^{15}	2.975	3.067	4.650×10^{15}	451.2	437.6
	-1,-1	4.663×10^{15}	3.001	3.094	4.640×10^{15}	448.2	434.8
	Avg.	4.693×10^{15}	2.969	3.061	4.670×10^{15}	450.3 ± 2.4	436.8 ± 2.3
B1.8B-2	-1,1	8.135×10^{15}	1.748	1.799	8.070×10^{15}	442.5	429.9
ρ_i = 1.79	0,1	8.035×10^{15}	1.772	1.823	7.971×10^{15}	441.9	429.5
NBS-4	1,1	7.913×10^{15}	1.775	1.827	7.850×10^{15}	447.9	435.2
D = 432.8	-1,0	8.052×10^{15}	1.764	1.814	7.988×10^{15}	442.9	430.7
	0,0	7.906×10^{15}	1.778	1.829	7.843×10^{15}	447.6	435.1
	1,0	7.971×10^{15}	1.775	1.826	7.907×10^{15}	444.7	432.3
	Avg.	8.002×10^{15}	1.769	1.820	7.938×10^{15}	444.6 ± 2.6	432.1 ± 2.5

Table 5 - Continued

Wafer Identification	Site	N cm^{-3}	$\rho_{23°C}$ Ω·cm	$\rho_{300\ K}$ Ω·cm	p cm^{-3}	$\mu_{23°C}$ $cm^2/V·s$	$\mu_{300\ K}$ $cm^2/V·s$
B1.1B-3	-1,1	1.312×10^{16}	1.141	1.173	1.297×10^{16}	421.8	410.2
ρ_i = 1.14	1,1	1.262×10^{16}	1.134	1.166	1.247×10^{16}	441.4	429.3
NBS-3	-2,0	1.281×10^{16}	1.132	1.164	1.266×10^{16}	435.5	423.5
D = 433.1	1,0	1.279×10^{16}	1.138	1.170	1.264×10^{16}	433.9	422.0
	2,0	1.281×10^{16}	1.146	1.178	1.266×10^{16}	430.2	418.5
	0,-1	1.270×10^{16}	1.132	1.164	1.255×10^{16}	439.3	427.3
	Avg.	1.281×10^{16}	1.137	1.169	1.266×10^{16}	433.7 ± 7.0	421.8 ± 6.9
B0.81B-1	-1,2	1.908×10^{16}	0.813	0.835	1.874×10^{16}	409.7	398.9
ρ_i = 0.81	0,2	1.908×10^{16}	0.805	0.827	1.874×10^{16}	413.7	402.7
NBS-4	1,2	1.886×10^{16}	0.802	0.824	1.852×10^{16}	420.2	409.0
D = 433.3	-1,1	1.901×10^{16}	0.800	0.822	1.867×10^{16}	417.9	406.7
	1,1	1.855×10^{16}	0.810	0.832	1.822×10^{16}	422.9	411.7
	0,0	1.896×10^{16}	0.802	0.824	1.862×10^{16}	418.0	407.0
	1,0	1.909×10^{16}	0.814	0.836	1.875×10^{16}	408.9	398.2
	-1,-1	1.871×10^{16}	0.810	0.832	1.837×10^{16}	419.5	408.4
	Avg.	1.892×10^{16}	0.807	0.829	1.858×10^{16}	416.4 ± 5.1	405.3 ± 4.9
D0.58B-2	-2,0	2.890×10^{16}	0.5718	0.5867	2.818×10^{16}	387.3	377.5
ρ_i = 0.58	0,0	2.877×10^{16}	0.5723	0.5872	2.805×10^{16}	388.8	378.9
NBS-3	1,0	2.897×10^{16}	0.5713	0.5862	2.825×10^{16}	386.7	376.9
D = 433.6	-2,-1	2.870×10^{16}	0.5777	0.5927	2.799×10^{16}	386.0	376.2
	-1,-1	2.906×10^{16}	0.5718	0.5867	2.834×10^{16}	385.2	375.4
	1,-1	2.922×10^{16}	0.5677	0.5825	2.849×10^{16}	385.9	376.1
	Avg.	2.894×10^{16}	0.5721	0.5870	2.822×10^{16}	386.7 ± 1.3	376.8 ± 1.2
E0.43B-3	-1,1	4.196×10^{16}	0.4068	0.4165	4.053×10^{16}	378.6	369.7
ρ_i = 0.43	0,1	4.311×10^{16}	0.4104	0.4202	4.164×10^{16}	365.2	356.7
NBS-4	1,1	4.215×10^{16}	0.4072	0.4169	4.071×10^{16}	376.5	367.7
D = 433.8	-1,0	4.196×10^{16}	0.4078	0.4175	4.053×10^{16}	377.6	368.9
	0,0	4.139×10^{16}	0.4179	0.4279	3.998×10^{16}	373.6	364.8
	1,0	4.109×10^{16}	0.4071	0.4168	3.969×10^{16}	386.3	377.3
	Avg.	4.194×10^{16}	0.4095	0.4193	4.051×10^{16}	376.3 ± 6.9	367.5 ± 6.7
B0.32B-2	-1,1	5.927×10^{16}	0.3085	0.3154	5.661×10^{16}	357.4	349.6
ρ_i = 0.32	0,1	5.861×10^{16}	0.3136	0.3206	5.598×10^{16}	355.5	347.8
NBS-4	1,1	5.878×10^{16}	0.3144	0.3214	5.614×10^{16}	353.6	345.9
D = 433.8	-1,0	5.987×10^{16}	0.3105	0.3174	5.718×10^{16}	351.5	343.9
	0,0	5.944×10^{16}	0.3096	0.3165	5.677×10^{16}	355.1	347.4
	1,0	5.911×10^{16}	0.3096	0.3165	5.645×10^{16}	357.1	349.3
	Avg.	5.918×10^{16}	0.3110	0.3180	5.646×10^{16}	355.0 ± 2.2	347.3 ± 2.1
B0.23B-2	-1,1	9.020×10^{16}	0.2216	0.2261	8.461×10^{16}	332.9	326.3
ρ_i = 0.22	0,1	8.890×10^{16}	0.2236	0.2282	8.339×10^{16}	334.7	328.0
NBS-4	1,1	8.791×10^{16}	0.2213	0.2258	8.246×10^{16}	342.0	335.2
D = 433.8	-1,0	8.775×10^{16}	0.2234	0.2280	8.231×10^{16}	339.4	332.6
	0,0	8.783×10^{16}	0.2241	0.2287	8.239×10^{16}	338.0	331.2
	1,0	9.166×10^{16}	0.2161	0.2205	8.598×10^{16}	335.9	329.2
	Avg.	8.904×10^{16}	0.2217	0.2262	8.352×10^{16}	337.2 ± 3.3	330.4 ± 3.2
B0.17B-1	-1,1	1.369×10^{17}	0.1585	0.1614	1.254×10^{17}	314.0	308.4
ρ_i = 0.165	0,1	1.366×10^{17}	0.1604	0.1634	1.252×10^{17}	310.8	305.1
NBS-4	1,1	1.338×10^{17}	0.1603	0.1633	1.226×10^{17}	317.6	311.8
D = 433.8	-1,0	1.377×10^{17}	0.1588	0.1617	1.262×10^{17}	311.4	305.9
	0,0	1.395×10^{17}	0.1586	0.1615	1.278×10^{17}	307.9	302.4
	1,0	1.397×10^{17}	0.1595	0.1624	1.280×10^{17}	305.7	300.3
	Avg.	1.374×10^{17}	0.1594	0.1623	1.259×10^{17}	311.2 ± 4.2	305.6 ± 4.1

Table 5 - Continued

Wafer Identification	Site	N cm^{-3}	$\rho_{23°C}$ Ω·cm	$\rho_{300\ K}$ Ω·cm	p cm^{-3}	$\mu_{23°C}$ $cm^2/V·s$	$\mu_{300\ K}$ $cm^2/V·s$
B0.097B-2	-1,1	2.717×10^{17}	0.0968	0.0982	2.355×10^{17}	273.8	269.9
ρ_i = 0.096	0,1	1.895×10^{17}	0.0952	0.0966	2.509×10^{17}	261.3	257.5
NBS-4	1,1	2.935×10^{17}	0.0942	0.0955	2.544×10^{17}	260.4	256.9
D = 433.8	-1,0	2.848×10^{17}	0.0954	0.0968	2.469×10^{17}	265.0	261.1
	0,0	2.910×10^{17}	0.0945	0.0958	2.522×10^{17}	261.9	258.3
	1,0	2.862×10^{17}	0.0942	0.0955	2.481×10^{17}	267.1	263.4
	Avg.	2.861×10^{17}	0.0951	0.0964	2.480×10^{17}	264.9 ± 5.0	261.2 ± 4.9
B0.090B-2	-1,3	3.189×10^{17}	0.0889	0.0901	2.742×10^{17}	256.0	252.6
ρ_i = 0.090	0,3	3.242×10^{17}	0.0891	0.0903	2.788×10^{17}	251.3	247.9
NBS-3	-2,2	3.132×10^{17}	0.0893	0.0905	2.693×10^{17}	259.5	256.1
D = 433.6	0,2	3.210×10^{17}	0.0893	0.0905	2.760×10^{17}	253.2	249.9
	1,2	3.147×10^{17}	0.0891	0.0903	2.706×10^{17}	258.9	255.4
	0,1	3.200×10^{17}	0.0890	0.0902	2.752×10^{17}	254.8	251.4
	1,1	3.219×10^{17}	0.0890	0.0902	2.768×10^{17}	253.4	250.0
	Avg.	3.191×10^{17}	0.0891	0.0903	2.744×10^{17}	255.3 ± 3.0	251.9 ± 3.0
B0.054B-3	-1,1	7.260×10^{17}	0.0548	0.0553	5.757×10^{17}	197.8	196.0
ρ_i = 0.055	0,1	7.183×10^{17}	0.0548	0.0553	5.696×10^{17}	200.0	198.1
NBS-4	1,1	7.016×10^{17}	0.0553	0.0558	5.563×10^{17}	202.9	201.1
D = 433.8	1,0	7.159×10^{17}	0.0549	0.0554	5.677×10^{17}	200.3	198.5
	-1,-1	7.128×10^{17}	0.0546	0.0551	5.652×10^{17}	202.2	200.4
	0,-1	7.109×10^{17}	0.0546	0.0551	5.637×10^{17}	202.8	200.9
	1,-1	7.318×10^{17}	0.0546	0.0551	5.803×10^{17}	197.0	195.2
	Avg.	7.168×10^{17}	0.0548	0.0553	5.684×10^{17}	200.4 ± 2.4	198.6 ± 2.4

Table 6. Data for Silicon Slices with the Boron Density Determined by the Nuclear Track Technique.

Slice Identification	Run	N cm^{-3}	$\rho_{23°C}$ Ω·cm	$\rho_{300\ K}$ Ω·cm	p cm^{-3}	$\mu_{23°C}$ $cm^2/V·s$	$\mu_{300\ K}$ $cm^2/V·s$
A7	1	1.02×10^{15}	10.9	11.2	1.02×10^{15}	561	546
	2	1.33×10^{15}	10.9	11.2	1.33×10^{15}	431	419
	Avg.	1.18×10^{15}	10.9	11.2	1.18×10^{15}	496	482
521-5	1	1.84×10^{15}	10.8	11.1	1.84×10^{15}	314	306
	2	1.76×10^{15}	10.8	11.1	1.76×10^{15}	328	320
	3	1.71×10^{15}	10.8	11.1	1.71×10^{15}	338	329
	Avg.	1.77×10^{15}	10.8	11.1	1.77×10^{15}	327	318
521-22	1	5.01×10^{15}	3.08	3.17	4.99×10^{15}	406	395
	2	4.90×10^{15}	3.01	3.10	4.88×10^{15}	425	413
	Avg.	4.95×10^{15}	3.04	3.13	4.93×10^{15}	415	404
521-21	1	6.89×10^{15}	1.85	1.90	6.84×10^{15}	493	480
A6	1	7.17×10^{15}	1.84	1.89	7.11×10^{15}	477	465
521-53	1	2.26×10^{15}	0.71	0.73	2.21×10^{15}	398	387
	2	2.26×10^{15}	0.71	0.73	2.21×10^{15}	398	387
	3	2.27×10^{15}	0.71	0.73	2.22×10^{15}	396	385
	Avg.	2.26×10^{15}	0.71	0.73	2.21×10^{15}	397	386
521-4	1	6.00×10^{15}	0.28	0.29	5.72×10^{15}	390	376
	2	6.10×10^{15}	0.277	0.283	5.82×10^{15}	387	379
	Avg.	6.05×10^{15}	0.28	0.29	5.77×10^{15}	388	377
521-76	1	1.29×10^{17}	0.221	0.225	1.19×10^{17}	237	233
	2	1.12×10^{17}	0.221	0.225	1.03×10^{17}	274	269
	Avg.	1.21×10^{17}	0.221	0.225	1.11×10^{17}	225	251
521-57	1	4.55×10^{17}	0.0959	0.0972	3.78×10^{17}	172.2	169.9
	2	4.48×10^{17}	0.0959	0.0972	3.72×10^{17}	175.0	172.6
	Avg.	4.52×10^{17}	0.0959	0.0972	3.75×10^{17}	173.6	171.2
521-62	1	7.29×10^{17}	0.054	0.0545	5.78×10^{17}	200.0	198.2
	2	6.67×10^{17}	0.0558	0.0563	5.29×10^{17}	211.5	209.6
	3	7.41×10^{17}	0.0558	0.0563	5.88×10^{17}	190.3	188.6
	Avg.†	7.12×10^{17}	0.0552	0.0557	5.65×10^{17}	200.6	198.8
521-58	1	4.24×10^{18}	0.0204	0.0204	4.24×10^{18}	72.2	72.2
	2	3.89×10^{18}	0.0204	0.0204	3.89×10^{18}	78.7	78.7
	Avg.	4.06×10^{18}	0.0204	0.0204	4.06×10^{18}	75.5	75.5
A3	1†	5.17×10^{18}	0.0149	0.0149	5.17×10^{18}	81.0	81.0
521-44	1	5.96×10^{18}	0.0130	0.0130	5.96×10^{18}	80.6	80.6
	2	5.80×10^{18}	0.0130	0.0130	5.80×10^{18}	82.8	82.8
	Avg.	5.88×10^{18}	0.0130	0.0130	5.88×10^{18}	81.7	81.7

†Used for computer curve fit.

Table 6 - Continued

Slice Identification	Run	N cm^{-3}	$\rho_{23°C}$ Ω·cm	$\rho_{300\ K}$ Ω·cm	p cm^{-3}	$\mu_{23°C}$ $cm^2/V·s$	$\mu_{300\ K}$ $cm^2/V·s$
521-23	1	2.27×10^{19}	0.0047	0.0047	2.27×10^{19}	58.5	58.5
	2	2.14×10^{19}	0.0047	0.0047	2.14×10^{19}	62.1	62.1
	3	2.10×10^{19}	0.0047	0.0047	2.10×10^{19}	63.2	63.2
	Avg.†	2.17×10^{19}	0.0047	0.0047	2.17×10^{19}	61.3	61.3
A2	1	2.89×10^{19}	0.0040	0.0040	2.89×10^{19}	54.0	54.0
	2	2.81×10^{19}	0.0040	0.0040	2.81×10^{19}	55.5	55.5
	3	2.58×10^{19}	0.0040	0.0040	2.58×10^{19}	60.5	60.5
	4	2.82×10^{19}	0.0040	0.0040	2.82×10^{19}	55.3	55.3
	Avg.†	2.78×10^{19}	0.0040	0.0040	2.78×10^{19}	56.3	56.3
521-45	1	2.80×10^{19}	0.00294	0.00294	2.80×10^{19}	75.8	75.8
521-73	1	4.42×10^{19}	0.00176	0.00177	4.42×10^{19}	80.2	79.8
	2	4.53×10^{19}	0.00176	0.00177	4.53×10^{19}	78.3	77.9
	Avg.	4.47×10^{19}	0.00176	0.00177	4.47×10^{19}	79.2	78.8
521-24	1	1.00×10^{20}	0.00105	0.00106	1.00×10^{20}	59.4	58.9
	2	1.23×10^{20}	0.00105	0.00106	1.23×10^{20}	48.3	47.9
	3	1.23×10^{20}	0.00105	0.00106	1.23×10^{20}	48.3	47.9
	Avg.†	1.15×10^{20}	0.00105	0.00106	1.15×10^{20}	52.0	51.6

†Used for computer curve fit.

Table 7. Data for Boron-Doped Silicon Obtained from van der Pauw Specimens.

Specimen No.	T = 23°C				T = 300 K			
	R_H(cm^3/C)	p(cm^{-3})	ρ(Ω·cm)	μ(cm^2/V·s)	R_H(cm^3/C)	p(cm^{-3})	ρ(Ω·cm)	μ(cm^2/V·s)
B0.010B-1	0.5839	8.550×10^{18}	0.009625	75.8	0.5823	8.57×10^{18}	0.009637	75.6
E0.0092B-1	0.5175	9.650×10^{18}	0.008865	73.0	0.5165	9.67×10^{18}	0.008873	72.7
A0.0082B-1	0.4455	1.121×10^{19}	0.00798	69.8	0.4465	1.118×10^{19}	0.00800	69.8
E0.0077B-2	0.4044	1.235×10^{19}	0.00739	68.4	0.4041	1.236×10^{19}	0.00741	68.1
A0.0072B-2	0.3788	1.318×10^{19}	0.007064	67.0	0.3784	1.320×10^{19}	0.007080	66.8
E0.0064B-1	0.3163	1.579×10^{19}	0.006083	65.0	0.3153	1.584×10^{19}	0.006100	64.6
A0.0061B-1	0.3037	1.644×10^{19}	0.005932	64.0	0.3020	1.653×10^{19}	0.005949	63.5
A0.0059B-1	0.2883	1.732×10^{19}	0.005710	63.1	0.2881	1.733×10^{19}	0.005727	62.9
A0.0059B-1C†	0.2927	1.706×10^{19}	0.005830	62.8	0.2915	1.713×10^{19}	0.005845	62.3
Avg.	0.2905	1.719×10^{19}	0.005770	63.0	0.2898	1.723×10^{19}	0.005786	62.6
0.005B-R7370	0.2572	1.941×10^{19}	0.00510	63.1	0.2560	1.950×10^{19}	0.005145	62.2
0.0043B-23-1	0.2030	2.460×10^{19}	0.00424	59.8	0.2047	2.439×10^{19}	0.00426	60.1
0.0030B-45-1	0.1305	3.826×10^{19}	0.002851	57.2	0.1304	3.829×10^{19}	0.002866	56.9
B0.0019B-2	0.0821	6.080×10^{19}	0.001849	55.5	0.0826	6.045×10^{19}	0.001862	55.5
0.0018B-73-1	0.0750	6.660×10^{19}	0.001701	55.1	0.0743	6.720×10^{19}	0.001712	54.3
0.0018B-73-1C†	0.0751	6.650×10^{19}	0.001712	54.8	0.0752	6.640×10^{19}	0.001723	54.6
Avg.	0.0750	6.655×10^{19}	0.001707	55.0	0.0747	6.680×10^{19}	0.001718	54.4
0.0010B-24-1	0.0449	1.112×10^{20}	0.001047	53.6	0.0446	1.120×10^{20}	0.001054	52.9
0.0010B-74-1	0.0446	1.120×10^{20}	0.001036	53.8	0.0449	1.112×10^{20}	0.001043	53.8
(repeat)	0.0447	1.117×10^{20}	0.001033	54.1	0.0448	1.115×10^{20}	0.001040	53.8
0.0010B-74-1C†	0.0446	1.120×10^{20}	0.001027	54.3	0.0444	1.125×10^{20}	0.001034	53.7
Avg.	0.0446	1.119×10^{20}	0.001032	54.1	0.0447	1.117×10^{20}	0.001039	53.8
A0.00087B-1	0.0367	1.361×10^{20}	0.000851	53.9	0.0360	1.387×10^{20}	0.000857	52.5

†"C" denotes specimen in the shape of a Greek cross; all other specimens had shape shown in figure 3.

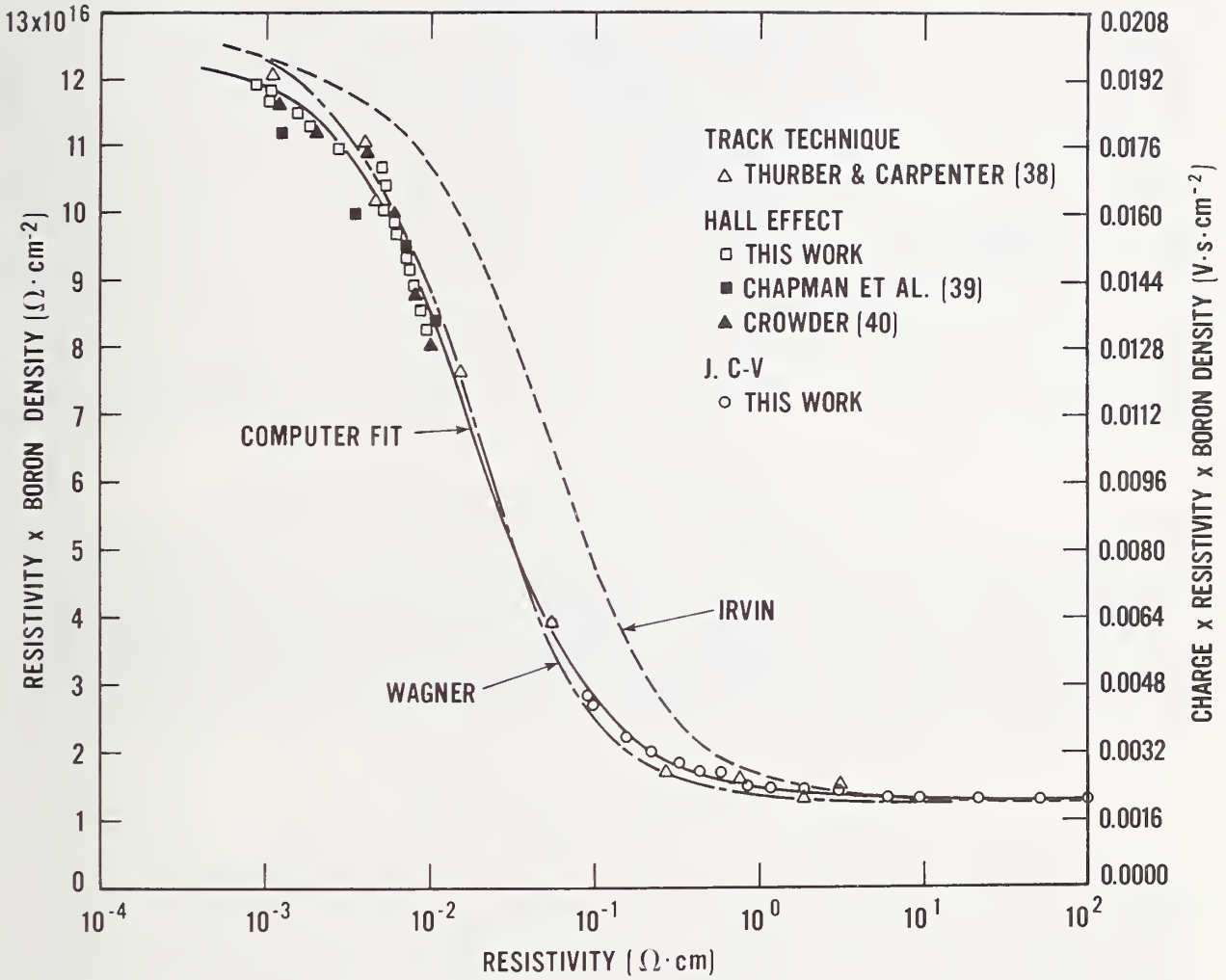

Figure 7. Resistivity-dopant density product as a function of resistivity at 300 K for boron-doped silicon. The junction capacitance voltage and Hall effect measurements are compared with the published work of Thurber and Carpenter [38], Chapman *et al.* [39], Crowder [40], Irvin [2], and Wagner [4]. The solid curve is an analytical fit to portions of these data as discussed in the text. Values of the product $q\rho N$ are on the right ordinate.

agreement with both the Hall effect and the C-V data. The curves shown are the Irvin relationship for p-type silicon, the Wagner relationship for boron-implanted silicon, and an analytical curve fit to the data given in tables 5, 6, and 7. As is evident from the figure, the results obtained from measurements on boron-doped silicon depart considerably from the p-type Irvin curve.

Figure 8 is a plot of hole mobility as a function of hole density at 300 K. The fairly recent data of Tsao and Sah [41] are significantly lower than the data of this work. This may result from the fact that back-surface contact resistance can strongly affect resistivity values obtained from the spreading resistance structure used by Tsao and Sah. The Caughey and Thomas [1] curve is a fit to the Irvin relationship with the assumption that the hole density equals the dopant density. The same assumption was used to obtain the Wagner curve; however, it was not a point-by-point determination but simply a change in one parameter of the Caughey and Thomas expression as required to fit data on boron-implanted silicon. Just as the Irvin curve is a poor fit to the resistivity-dopant density data of this work, the Caughey and Thomas expression is a poor fit to the mobility data. The Wagner expression is considerably better, but there are still noticeable deviations with respect to the experimental data. The theoretical calculation of Li [37] in figure 8, valid for densities less than 3×10^{18} cm^{-3}, is in excellent agreement with the C-V data of this work.

7. COMPUTER CURVE FITS FOR PHOSPHORUS-DOPED SILICON

The curve fits of the data were done using the DATAPLOT language [42] for the nonlinear least squares fitting. The simplest expression which gave a fit of the same precision as the uncertainty in the experimental data was the log of the resistivity-dopant density product equal to a third-degree polynominal divided by a third-degree polynominal. Therefore, the equation for fitting the resistivity-dopant density product was taken to have the form

$$\log_{10}(P/P_o) = \frac{A_0 + A_1X + A_2X^2 + A_3X^3}{1 + B_1X + B_2X^2 + B_3X^3}, \qquad (1)$$

with $P = q\rho N$ where q is the electronic charge,* ρ is the resistivity, and N is the electrically active dopant density. The normalization factor, P_o, was taken equal to 1 V·s/cm^2. Fits were made for both $X = \log_{10}(\rho/\rho_0)$ and $X = \log_{10}(N/N_0)$ with $\rho_0 = 1\ \Omega\cdot cm$ and $N_0 = 10^{16}$ cm^{-3}. With the use of the normalizing values, ρ_o and N_o, the magnitude of X is almost always less than 4. This is desirable from a computational standpoint because the computation is much less sensitive to the number of significant figures retained in the coefficients.

The data used for the curve fitting consisted of 26 points obtained from the C-V measurements, 12 points determined from the Hall effect measurements, 2 points from Esaki and Miyahara [43], and 1 point from Fair and Tsai [35]. The latter three points are listed in table 8 and were included to increase

* A value of 1.602×10^{-19} C was used for q in all of the curve fits; consequently, this is the appropriate value to use for subsequent calculations.

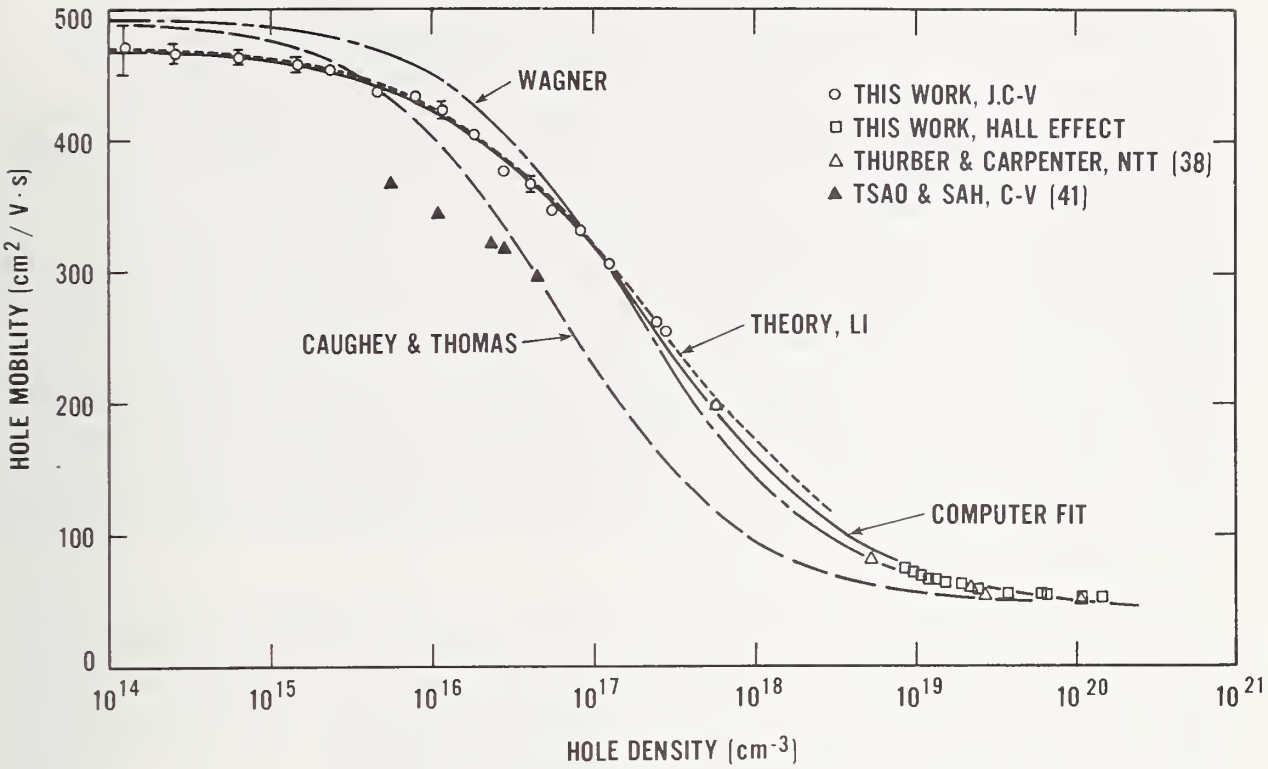

Figure 8. Hole mobility as a function of calculated hole density for boron-doped silicon at 300 K. All data points, except those in the heavily doped range, have been corrected for incomplete ionization using the work of Li [37]. The Caughey-Thomas [1] and Wagner [4] expressions were obtained without consideration of de-ionization and are plotted assuming equivalence of hole and dopant densities. This gives lower mobility in the range 10^{17} to 10^{19} cm^{-3}. The error bars on the C-V data of this work show the standard deviation calculated from the individual mobility values for that wafer. When not shown, the error bars lie within the plotted symbol.

Table 8. Miscellaneous Data for the Computer Curve Fits of Phosphorus-Doped Silicon.

Point No.	Source	N cm^{-3}	$\rho_{23°C}$ Ω·cm	$\rho_{300\ K}$ Ω·cm	n cm^{-3}	$\mu_{23°C}$ $cm^2/V·s$	$\mu_{300\ K}$ $cm^2/V·s$
1	experimental extrapolation	1×10^{12}	4276.0	4413.0	1×10^{12}	1460	1415
2	NAA/photometric	1.25×10^{18}	0.020	0.020	1.13×10^{18}	276	276
3	NAA/photometric	2.57×10^{18}	0.014	0.014	2.23×10^{18}	200	200
4	NAA/photometric	4.70×10^{18}	0.010	0.010	4.70×10^{18}	133	133
5	NAA/photometric	7.75×10^{18}	0.0073	0.0073	7.75×10^{18}	110	110
6	Esaki & Miyahara [43]	1.2×10^{20}†	0.00067	0.00067	1.2×10^{20}	78	78
7	Esaki & Miyahara [43]	1.6×10^{20}†	0.00055	0.00055	1.6×10^{20}	71	71
8	Fair & Tsai [35]	3×10^{20}†	0.000298	0.000298	3×10^{20}	*	*

†Electrically active dopant density assumed equal to electron density.
*Not included in mobility fit.

the range of the fit at high densities beyond that justified by the data of this work alone. In the region of the gap between the C-V and Hall effect data (phosphorus densities between 10^{18} and 10^{19} cm^{-3}), four resistivity-dopant density pairs were generated for the data base to be used in the curve fitting. These pairs, listed in table 8, were based on the NAA and photometric results, but actual values were chosen to give a smooth curve between the C-V and Hall effect data. In addition, a point was added at N = 1 x 10^{12} cm^{-3} to improve the fit for calculating values in the low dopant density range. This point was taken equal to the average of the four lowest dopant density data points since the ρN product is essentially constant in this region. Also, the inclusion of this point helps insure that the fits as a function of $\log_{10}(\rho/\rho_0)$ and $\log_{10}(N/N_0)$ both give essentially the same calculated values in this region. The coefficients for the fit of the data to eq (1) are given in table 9 for 23°C and 300 K. The table gives the approximate standard deviation for each coefficient and the residual standard deviation (R.S.D.) in units of volts-second per square centimeter. The R.S.D. is the square root of the quotient of the sum of the squared residuals,* divided by the number of degrees of freedom.

The plot of the data used for the curve fit, with the exception of the point at 10^{12} cm^{-3}, and the least squares fit of the $q\rho N$ product *versus* N for 300 K are shown in figure 9. This figure clearly shows that the "min-max" expressions of Caughey and Thomas [1] are not suitable for these data as there is no plateau or maximum at high dopant densities. The curve obtained for the product as a function of resistivity is plotted in figure 10.

The two expressions, one a function of $\log_{10}(\rho/\rho_0)$ and the other a function of $\log_{10}(N/N_0)$, have a worst case self-consistency of 8 percent for all values of N (and corresponding values of ρ) within the range 1 x 10^{12} to 4 x 10^{20} cm^{-3}. That is, when the product $q\rho N$ is calculated for a given N, giving a ρ which is used in the $q\rho N$ *versus* ρ expression to again calculate the product, the latter product will be within 8 percent of the former. The maximum difference occurs only in the low 10^{18} cm^{-3} range; elsewhere the fits are consistent within 4 percent. When the self-consistency is calculated starting with a given ρ, the fits have a maximum difference of 4 percent for resistivities from 2 x 10^{-4} to 3 x 10^{3} $\Omega \cdot cm$. The self-consistency is shown (solid curves) as a function of dopant density in figure 11 and as a function of resistivity in figure 12.

Curve fits were also obtained for electron mobility as a function of both electron density, n, and resistivity. It was found that better and more self-consistent fits were possible if the point at 3 x 10^{20} cm^{-3} were omitted. Otherwise the data used for the mobility fits corresponded to that used for the product fits. As mentioned previously, the percent ionization calculations of Li and Thurber [30] were used to obtain the electron density from the measured dopant density prior to the computation of mobility. The expression for calculating the electron mobility is of the form

$$\log_{10}(\mu/\mu_0) = \frac{A_0 + A_1X + A_2X^2 + A_3X^3}{1 + B_1X + B_2X^2 + B_3X^3}, \qquad (2)$$

* The difference between the measured point and the predicted value from the curve fit.

Table 9. Coefficients and Residual Standard Deviation (R.S.D.) for the Fit of the Product qρN for Phosphorus-Doped Silicon Using Eq (1).

Temp. X	23°C $\log_{10}(\rho/\rho_0)$	23°C $\log_{10}(N/N_0)$	300 K $\log_{10}(\rho/\rho_0)$	300 K $\log_{10}(N/N_0)$
A_0	-3.1083 ± 0.0038	-3.0769 ± 0.0027	-3.0951 ± 0.0037	-3.0652 ± 0.0026
A_1	-3.2626 ± 0.0952	2.2108 ± 0.0392	-3.2303 ± 0.0909	2.1853 ± 0.0415
A_2	-1.2196 ± 0.0341	-0.62272 ± 0.0159	-1.2024 ± 0.0325	-0.61080 ± 0.0170
A_3	-0.13923 ± 0.00468	0.057501 ± 0.00287	-0.13679 ± 0.00466	0.056189 ± 0.00327
B_1	1.0265 ± 0.0318	-0.68157 ± 0.0134	1.0205 ± 0.0305	-0.67642 ± 0.0141
B_2	0.38755 ± 0.0109	0.19833 ± 0.00507	0.38382 ± 0.0105	0.19542 ± 0.00541
B_3	0.041833 ± 0.00168	-0.018376 ± 0.000986	0.041338 ± 0.00169	-0.018100 ± 0.00112
R.S.D.	2.78×10^{-4}	2.21×10^{-4}	2.67×10^{-4}	2.09×10^{-4}

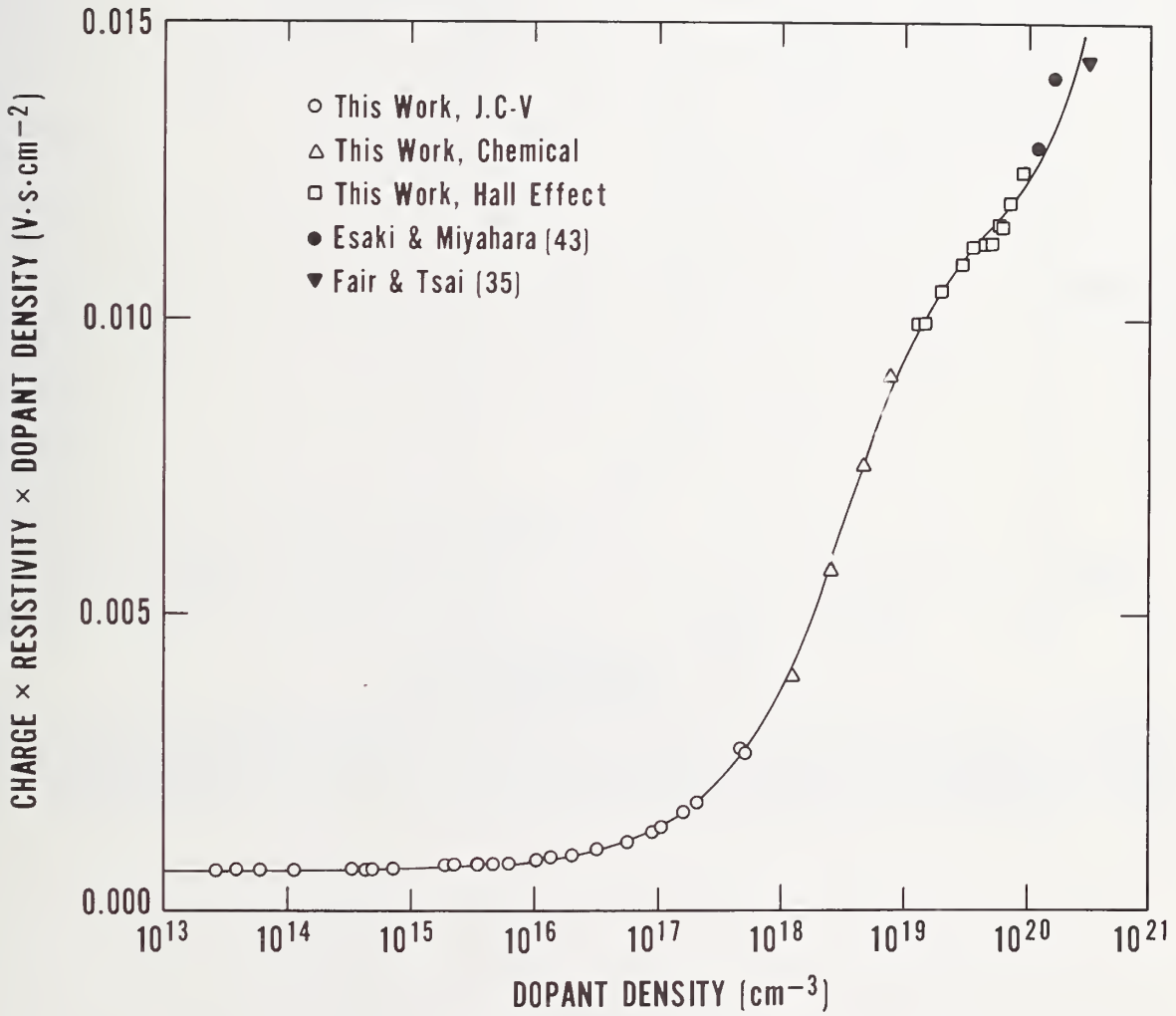

Figure 9. The qρN product as a function of dopant density for phosphorus-doped silicon at 300 K. The curve is the least squares fit to the data points shown using eq (1). Coefficients are given in table 9.

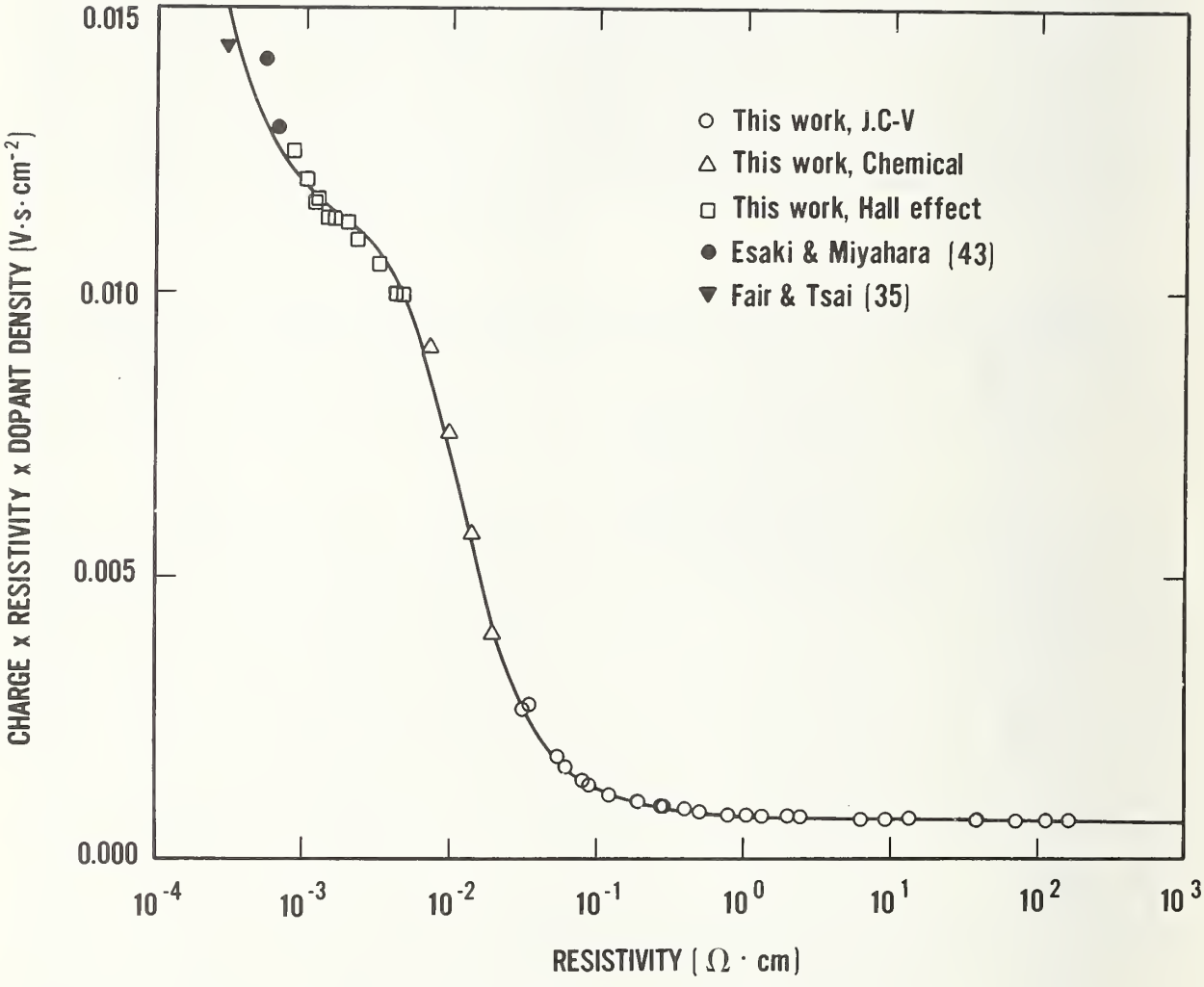

Figure 10. The qρN product as a function of resistivity for phosphorus-doped silicon at 300 K. Equation (1) was used as the form of the curve fit to the data points shown. Coefficients are given in table 9.

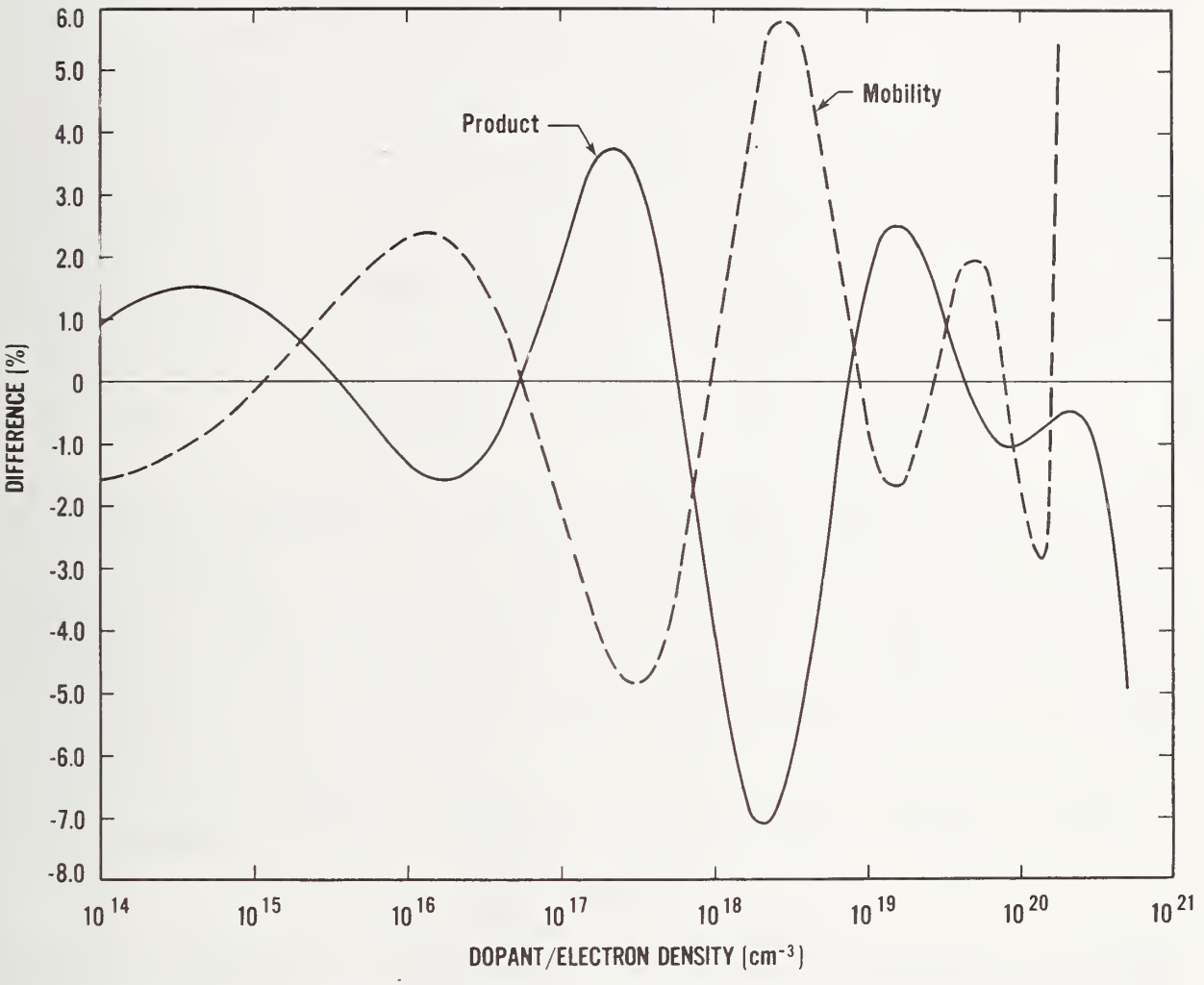

Figure 11. Self-consistency of the product and mobility fits at 23°C for phosphorus-doped silicon plotted *versus* dopant density for the product fits and *versus* electron density for the mobility fits. The procedure for calculating the difference is discussed in the text.

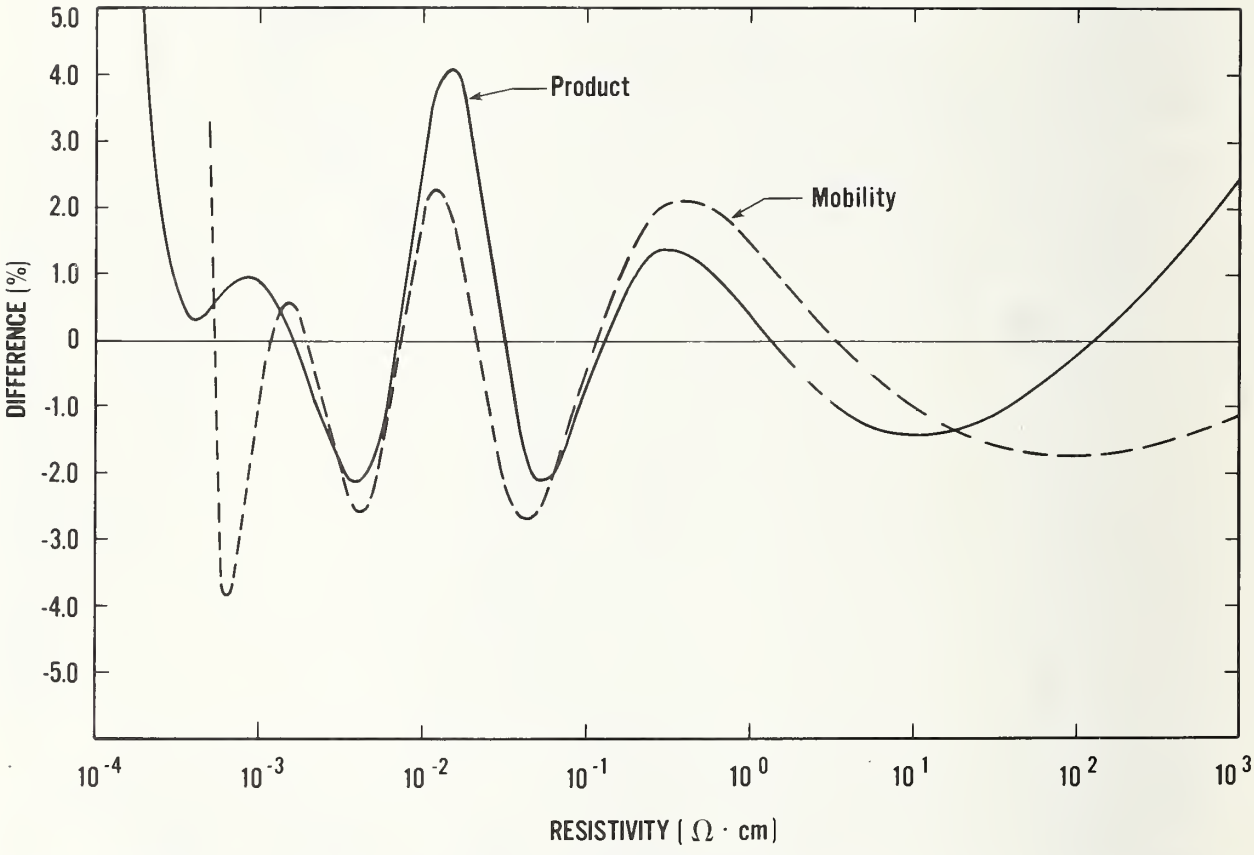

Figure 12. Self-consistency of the product and mobility fits at 23°C for phosphorus-doped silicon plotted *versus* resistivity. The procedure for calculating the difference is discussed in the text.

where μ is the mobility and $\mu_0 = 1\ cm^2/V \cdot s$. (In this equation, the A's and B's represent coefficients to be determined; they are not constants from previous fits.) As before, fits were made for both $X = \log_{10} (\rho/\rho_0)$ and $X = \log_{10} (n/n_0)$ for temperatures of 23°C and 300 K. Values for the coefficients are given in table 10. The plot of the mobility data and fitted curve as a function of resistivity for 300 K is given in figure 13. The fit of mobility *versus* electron density is shown in figures 5 and 6 for comparison with experimental data. An expression of the form suggested by Masetti and Solmi [36] was also tried for the mobility fits, but the percent residuals in the low mobility range were significantly larger than with eq (2), particularly for the fit as a function of resistivity.

The self-consistency of the mobility fits, plotted as dashed curves in figures 11 and 12, shows a maximum difference of 6 percent for electron densities in the range 10^{12} to $10^{20}\ cm^{-3}$. The expressions rapidly diverge for densities greater than $2 \times 10^{20}\ cm^{-3}$. The fit as a function of resistivity is the better choice for approximating mobility values beyond the range of the fitted data. When the self-consistency is calculated starting with a given resistivity, the fits have a maximum difference of 3 percent for resistivities from 6×10^{-4} to $10^4\ \Omega \cdot cm$. The self-consistency graphs shown are for 23°C; calculations for 300 K closely parallel those for 23°C.

8. COMPUTER CURVE FITS FOR BORON-DOPED SILICON

The previous expressions for the fits to phosphorus-doped silicon are in the form of quotients of two third-degree polynomials in order to fit the shape of the product and mobility curves at high phosphorus densities. However, for boron-doped silicon, the product is well behaved at very high densities, such that "min-max" relationships similar to those proposed by Caughey and Thomas [1] give satisfactory fits. Modifications are necessary for the fits of mobility as will be discussed later. These relationships have the advantage that two of the parameters, $(q\rho N)_{min}$ and $(q\rho N)_{max}$, have a readily identified physical significance in that they approximately equal the true limiting value of these quantities.

The expression for the product $q\rho N$ as a function of ρ was taken as

$$q\rho N = (q\rho N)_{min} + \frac{(q\rho N)_{max} - (q\rho N)_{min}}{1 + \left(\frac{\rho}{\rho_{ref}}\right)^{\alpha}}, \qquad (3)$$

where q is the electronic charge, N is the boron density, ρ is the resistivity, $(q\rho N)_{min}$ and $(q\rho N)_{max}$ are the asymptotic minimum and maximum values of the product, ρ_{ref} is a reference value corresponding to the resistivity for which the derivative of the product is a maximum, and α is a measure of the slope of the curve near the reference value. The data used for the fit, given in tables 5, 6, and 7, were the junction C-V and Hall effect results of this work, and selected NTT results for boron densities greater than $5 \times 10^{17}\ cm^{-3}$. The NTT data at lower densities were omitted because the data, while in general agreement with the C-V results, showed significantly more scatter. For high boron densities, the NTT results may be better than those from the Hall effect because of the need to assume a value for the Hall

Table 10. Coefficients and Residual Standard Deviation (R.S.D.) for the Fit of Electron Mobility for Phosphorus-Doped Silicon Using Eq (2).

Temp. X	23°C $\log_{10}(\rho/\rho_0)$	23°C $\log_{10}(n/n_0)$	300 K $\log_{10}(\rho/\rho_0)$	300 K $\log_{10}(n/n_0)$
A_0	3.1122 ± 0.0034	3.0746 ± 0.0025	3.0985 ± 0.0037	3.0629 ± 0.0025
A_1	3.3347 ± 0.0951	-2.2679 ± 0.0076	3.3257 ± 0.0923	-2.2522 ± 0.0077
A_2	1.2610 ± 0.0511	0.62998 ± 0.00245	1.2581 ± 0.0481	0.62327 ± 0.00249
A_3	0.15701 ± 0.0198	-0.061285 ± 0.00087	0.15679 ± 0.0189	-0.060415 ± 0.00087
B_1	1.0463 ± 0.0324	-0.70017 ± 0.00290	1.0485 ± 0.0317	-0.69851 ± 0.00292
B_2	0.39941 ± 0.0167	0.19839 ± 0.00113	0.40020 ± 0.0156	0.19716 ± 0.00114
B_3	0.049746 ± 0.00547	-0.020150 ± 0.00041	0.049883 ± 0.00512	-0.019950 ± 0.00041
R.S.D.	14.9	11.6	14.8	11.2

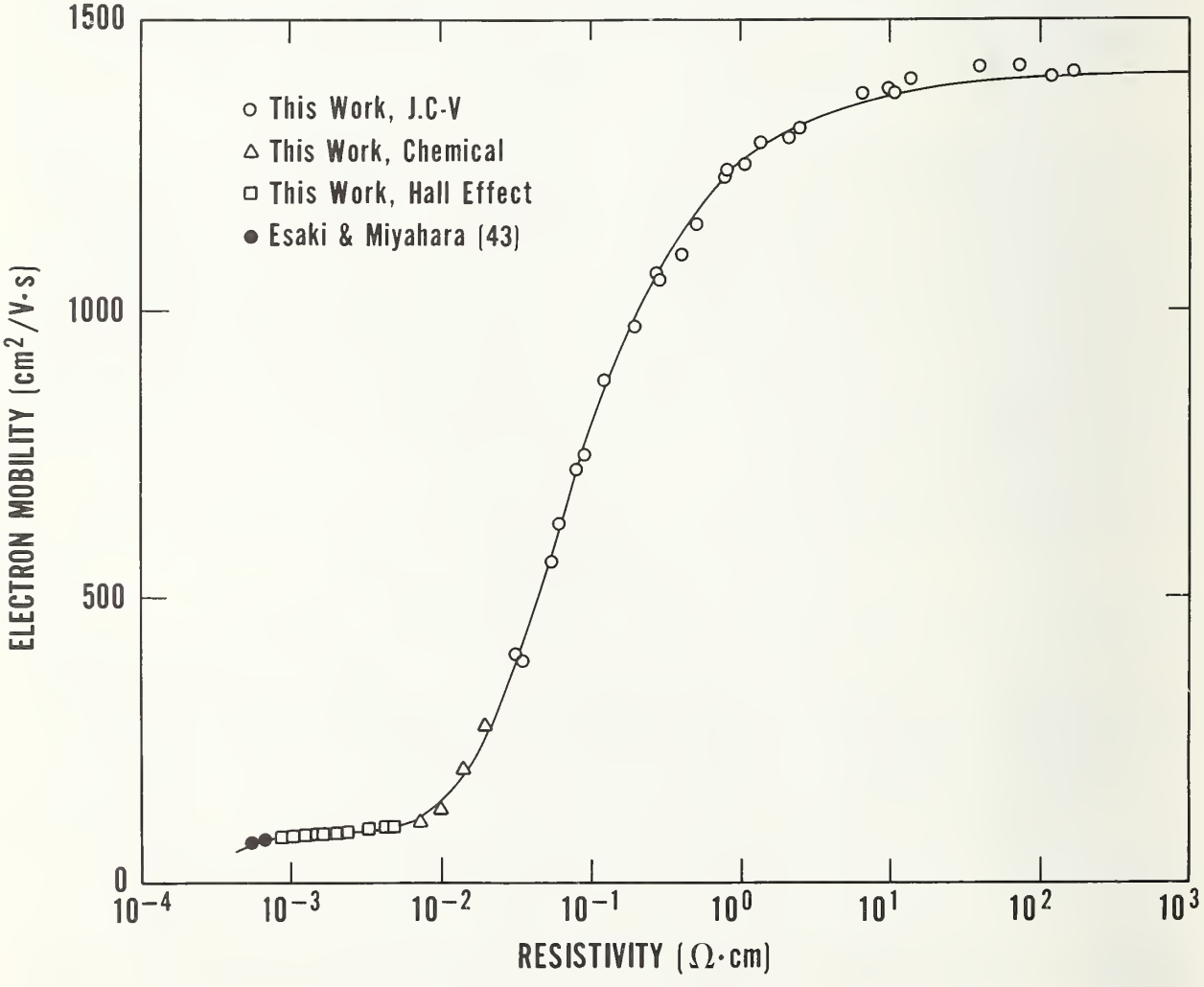

Figure 13. Electron mobility *versus* resistivity at 300 K for phosphorus-doped silicon. The curve is the least squares fit to the points using eq (2) with coefficients given in table 10.

factor in the latter case. This same set of 300 K data, and its counterpart at 23°C, was used for all of the curve fits. The resistivity values of the 39 fitted data points spanned the range 0.00085 to 100 Ω·cm with corresponding dopant densities between 1.4×10^{20} and 1.3×10^{14} cm^{-3}. The least-squares curve at 300 K is shown in figure 8 for comparison with experimental data and other curves. All four parameters as determined by the fit are given in table 11 for both 23°C and 300 K. The approximate standard deviation is given for each parameter in its own units, and the residual standard deviation (R.S.D.) for the fit is listed in units of $q\rho N$.

The expression for the product $q\rho N$ as a function of dopant density has the same form as eq (3) except for a negative value of the exponent because of the inverse relationship between ρ and N:

$$q\rho N = (q\rho N)_{min} + \frac{(q\rho N)_{max} - (q\rho N)_{min}}{1 + \left(\frac{N}{N_{ref}}\right)^{\alpha}} . \qquad (4)$$

(In this equation $(q\rho N)_{min}$, $(q\rho N)_{max}$, N_{ref}, and α represent the parameters to be determined; they are not constants from previous fits.) Values for the four parameters are listed in table 12 for both 23°C and 300 K. The curve for 300 K and the experimental data used to obtain it are shown in figure 14.

In comparing the product fits as a function of resistivity with those as a function of dopant density, it is evident that minimum and maximum values which should be correspondingly equal are somewhat different. This is, of course, a consequence of the independent fits where no parameters are fixed. The $(q\rho N)_{min}$ values differ by 2 percent and the fits differ by this same percentage at $N = 10^{14}$ cm^{-3}. The $(q\rho N)_{max}$ values differ by 4 percent; however, these are asymptotic values, and at the upper limit of the experimental data ($N \approx 10^{20}$ cm^{-3}) there is still considerable curvature. The difference between the fits in this region is less than 1 percent. The product fits are self-consistent within 3 percent for all dopant densities (and corresponding resistivities) in the range 10^{14} to 10^{20} cm^{-3}; see the solid curves in figures 15 and 16. That is, when the product $q\rho N$ is calculated for a given dopant density with eq (4), a resistivity is derived which can be used in the $q\rho N$ *versus* ρ expression [eq (3)] to again calculate the product. The latter product will be within 3 percent of the former.

Hole mobilities were calculated from resistivity and hole density values. Except in the heavily doped range, where hole density is assumed to equal dopant density, hole densities were obtained from dopant densities using the percent ionization calculations of Li [37]. A suitable expression for the hole mobility, μ_h, as a function of hole density, p, was found to be

$$\mu_h = A \exp(-p_c/p) + \frac{\mu_{max}}{1 + \left(\frac{p}{p_{ref}}\right)^{\alpha}} . \qquad (5)$$

This form gave a significantly better fit than the simpler form of the type used for fitting the product curves. The effect of the exponential factor in

Table 11 — Parameters and Residual Standard Deviation (R.S.D.) for the Fit of $q\rho N$ *versus* ρ for Boron-Doped Silicon Using Eq (3).

Temperature	23°C	300 K
$(q\rho N)_{min}$ ($V \cdot s/cm^2$)	0.00213 ± 0.00009	0.00220 ± 0.00009
$(q\rho N)_{max}$ ($V \cdot s/cm^2$)	0.01947 ± 0.00018	0.01973 ± 0.00017
ρ_{ref} ($\Omega \cdot cm$)	0.01833 ± 0.00067	0.01782 ± 0.00060
α	1.105 ± 0.035	1.086 ± 0.032
R.S.D. ($V \cdot s/cm^2$)	0.000292	0.000266

Table 12 — Parameters and Residual Standard Deviation (R.S.D.) for the Fit of $q\rho N$ *versus* N for Boron-Doped Silicon Using Eq (4).

Temperature	23°C	300 K
$(q\rho N)_{min}$ ($V \cdot s/cm^2$)	0.00209 ± 0.00009	0.00215 ± 0.00008
$(q\rho N)_{max}$ ($V \cdot s/cm^2$)	0.02024 ± 0.00024	0.02053 ± 0.00022
N_{ref} (cm^{-3})	$3.88 \times 10^{18} \pm 0.21 \times 10^{18}$	$4.09 \times 10^{18} \pm 0.20 \times 10^{18}$
α	-0.737 ± 0.024	-0.727 ± 0.021
R.S.D. ($V \cdot s/cm^2$)	0.000268	0.000240

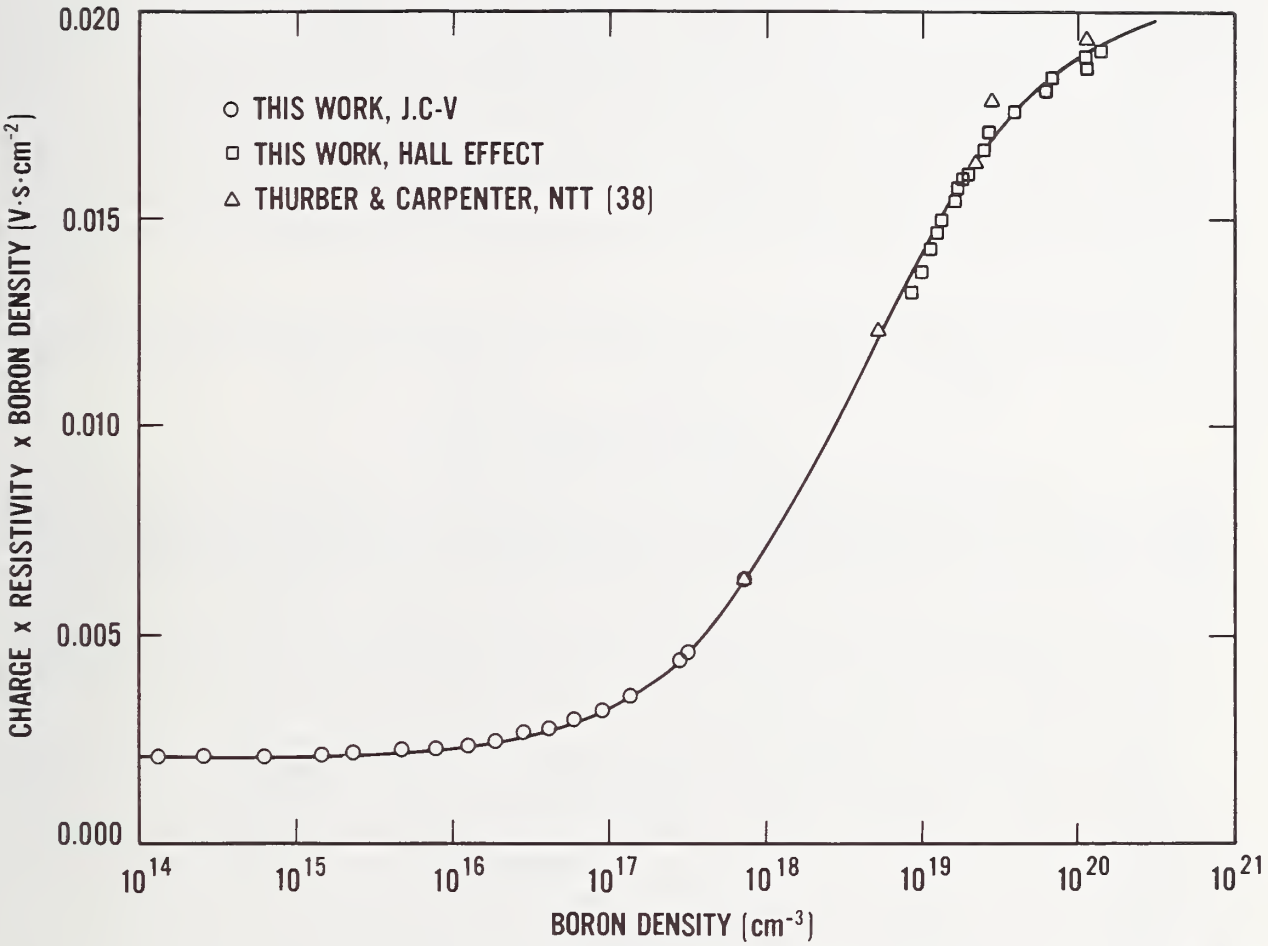

Figure 14. The qρN product as a function of boron density for 300 K. The curve is an analytical fit to the data points shown using eq (4). Parameter values are given in table 12.

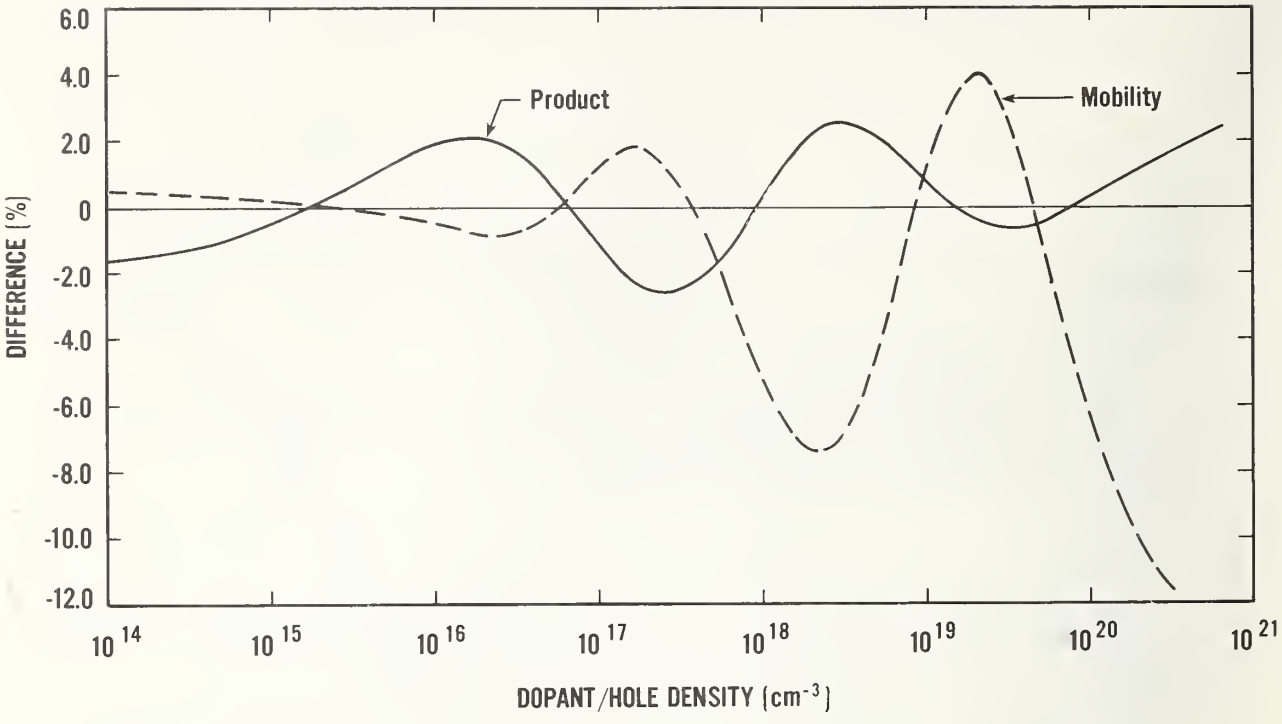

Figure 15. Self-consistency of the product and mobility fits at 23°C for boron-doped silicon plotted *versus* dopant density for the product fits and *versus* hole density for the mobility fits. The procedure for calculating the difference is discussed in the text.

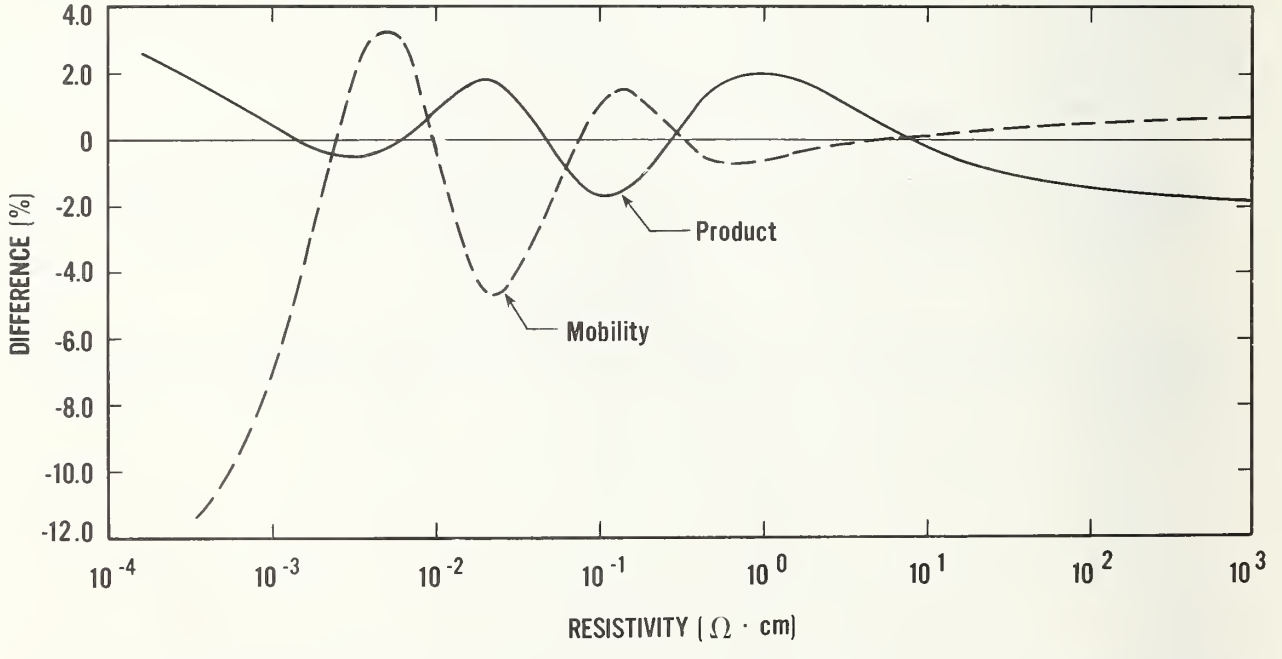

Figure 16. Self-consistency of the product and mobility fits at 23°C for boron-doped silicon plotted *versus* resistivity. The procedure for calculating the difference is discussed in the text.

the first term is to increase the mobility in the region of the curve where the dopant and hole densities deviate significantly from each other. The hole mobility approaches the constant value A for very large hole densities. The five parameters, determined by the fit to the 39 data points, are listed in table 13 for 23°C and 300 K. The curve for 300 K, calculated using the parameters in table 13, is shown in figure 8 for comparison with experimental data and other curves.

During the course of fitting the hole mobility to eq (5), it was found that convergence was obtained for two different values of p_c. Further work confirmed that there were two valleys, or local minima, for the variation of the R.S.D. with p_c, and the one located by the fitting procedure depended on the starting value for p_c. At 23°C one fit had $p_c = 9.00 \times 10^{16}$, A = 45.2, $\mu_{max} = 486.1$, $p_{ref} = 2.11 \times 10^{17}$, $\alpha = 0.718$, and R.S.D. = 3.18; the other had $p_c = 1.09 \times 10^{19}$, A = 41.4, $\mu_{max} = 492.5$, $p_{ref} = 3.06 \times 10^{17}$, $\alpha = 0.589$, and R.S.D. = 2.84. The former fit was selected in spite of its higher R.S.D. because it gave better self-consistency with the fit as a function of resistivity.

The form for the hole mobility as a function of resistivity was taken as

$$\mu_h = A \exp(-\rho/\rho_c) + \frac{\mu_{max}}{1 + \left(\frac{\rho}{\rho_{ref}}\right)^{\alpha}} . \qquad (6)$$

It was also found that the simple "min-max" form did not fit the mobility *versus* resistivity data well, particularly in the low resistivity range. The inclusion of the exponential in the first term improved the fit considerably. Its effect is similar to that of the exponential in eq (5). In this expression, the mobility is dominated by the first term at low resistivities and by the second term at high resistivities. The parameters determined by the fit are listed in table 14 for both 23°C and 300 K. The curve for 300 K and the experimental data used for the fit are shown in figure 17. The curve fits the shape of the experimental data very well at low resistivities so that extrapolation of eq (6), using the parameters in table 14, at the low resistivity end should give reasonable values. Thus, A can be considered to be approximately equal to the minimum value of the mobility. The mobility *versus* hole density fit is not as good at the low mobility end, as it is slightly below the data at $p = 10^{20}$ cm^{-3} and goes to a lower asymptotic value than is the case for eq (6). Consequently, an extrapolation of eq (5) at the low mobility end is less likely to be correct.

The μ_{max} values for the mobility fits as a function of hole density differ by about 0.7 percent from the μ_{max} values for the fits as a function of resistivity. The mobility fits are self-consistent within 2 percent for all hole densities (and corresponding resistivities) in the range 10^{14} to 5×10^{17} cm^{-3}; see the dashed curves in figures 15 and 16. In the 10^{18} cm^{-3} range, there are differences of up to 8 percent. The self-consistency improves in the low 10^{19} cm^{-3} range but increases again to 6 percent at 10^{20} cm^{-3} as the fits depart for very heavy doping.

The results of this work are incorporated in the ASTM document F 723 entitled "Practice for the Conversion Between Resistivity and Dopant Density for

Table 13 — Parameters and Residual Standard Deviation (R.S.D.) for the Fit of μ_h *versus* p Using Eq (5).

Temperature	23°C	300 K
A ($cm^2/V \cdot s$)	45.2 $\pm$ 1.3	44.9 $\pm$ 1.2
p_c (cm^{-3})	$9.00 \times 10^{16} \pm 2.3 \times 10^{16}$	$9.23 \times 10^{16} \pm 2.3 \times 10^{16}$
μ_{max} ($cm^2/V \cdot s$)	486.1 $\pm$ 1.9	470.5 $\pm$ 1.8
p_{ref} (cm^{-3})	$2.11 \times 10^{17} \pm 0.09 \times 10^{17}$	$2.23 \times 10^{17} \pm 0.10 \times 10^{17}$
α	0.718 $\pm$ 0.013	0.719 $\pm$ 0.013
R.S.D. ($cm^2/V \cdot s$)	3.18	3.07

Table 14 — Parameters and Residual Standard Deviation (R.S.D.) for the Fit of μ_h *versus* ρ Using Eq (6).

Temperature	23°C	300 K
A ($cm^2/V \cdot s$)	52.4 $\pm$ 3.8	51.6 $\pm$ 3.7
ρ_c ($\Omega \cdot cm$)	0.00409 $\pm$ 0.00077	0.00406 $\pm$ 0.00077
μ_{max} ($cm^2/V \cdot s$)	482.8 $\pm$ 2.4	467.3 $\pm$ 2.4
ρ_{ref} ($\Omega \cdot cm$)	0.0825 $\pm$ 0.0020	0.0794 $\pm$ 0.0019
α	-0.811 $\pm$ 0.018	-0.808 $\pm$ 0.019
R.S.D. ($cm^2/V \cdot s$)	4.89	4.78

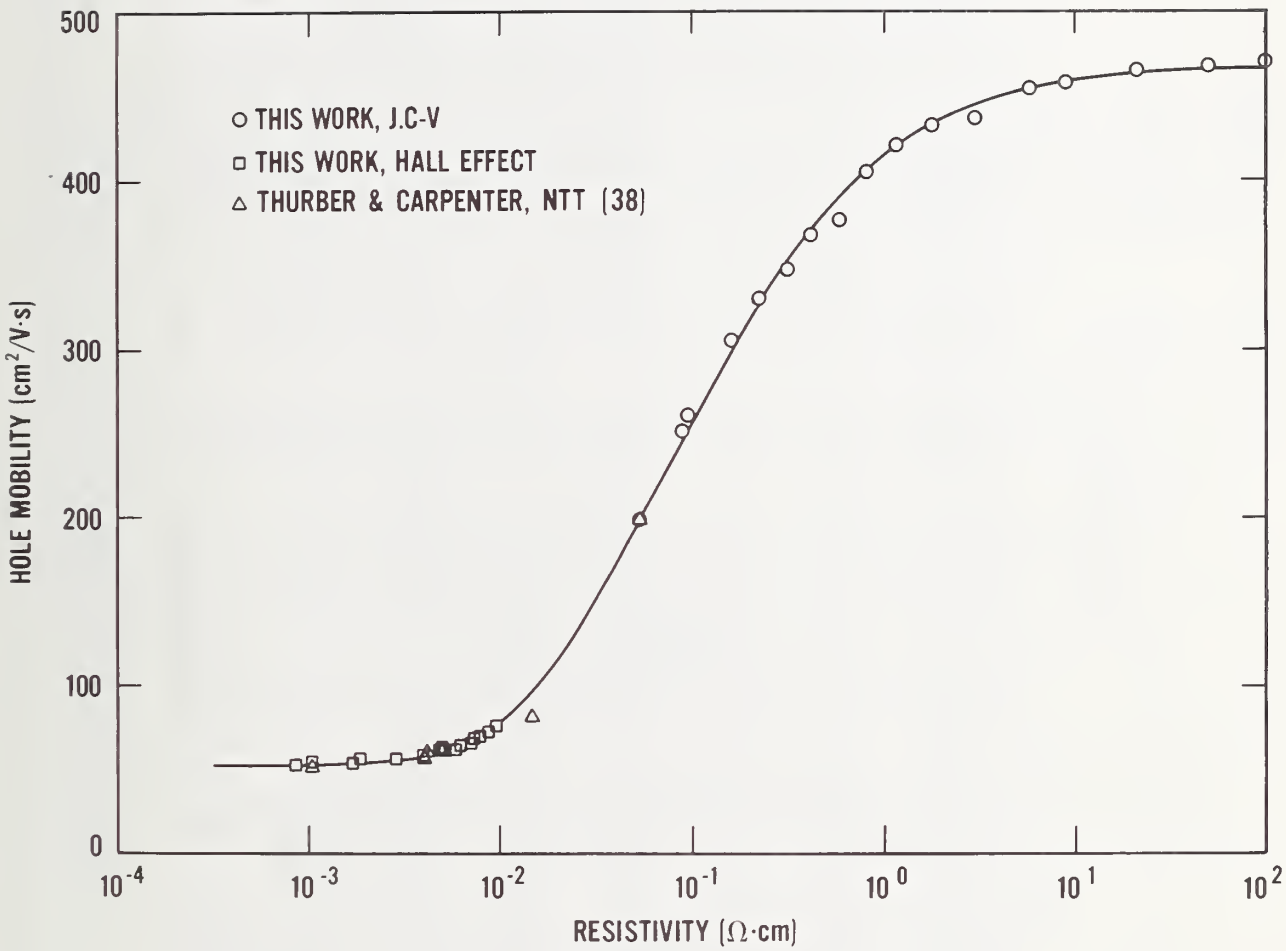

Figure 17. Hole mobility *versus* resistivity at 300 K for boron-doped silicon. The curve is an analytical fit to the data points shown using eq (6). Parameter values are given in table 14.

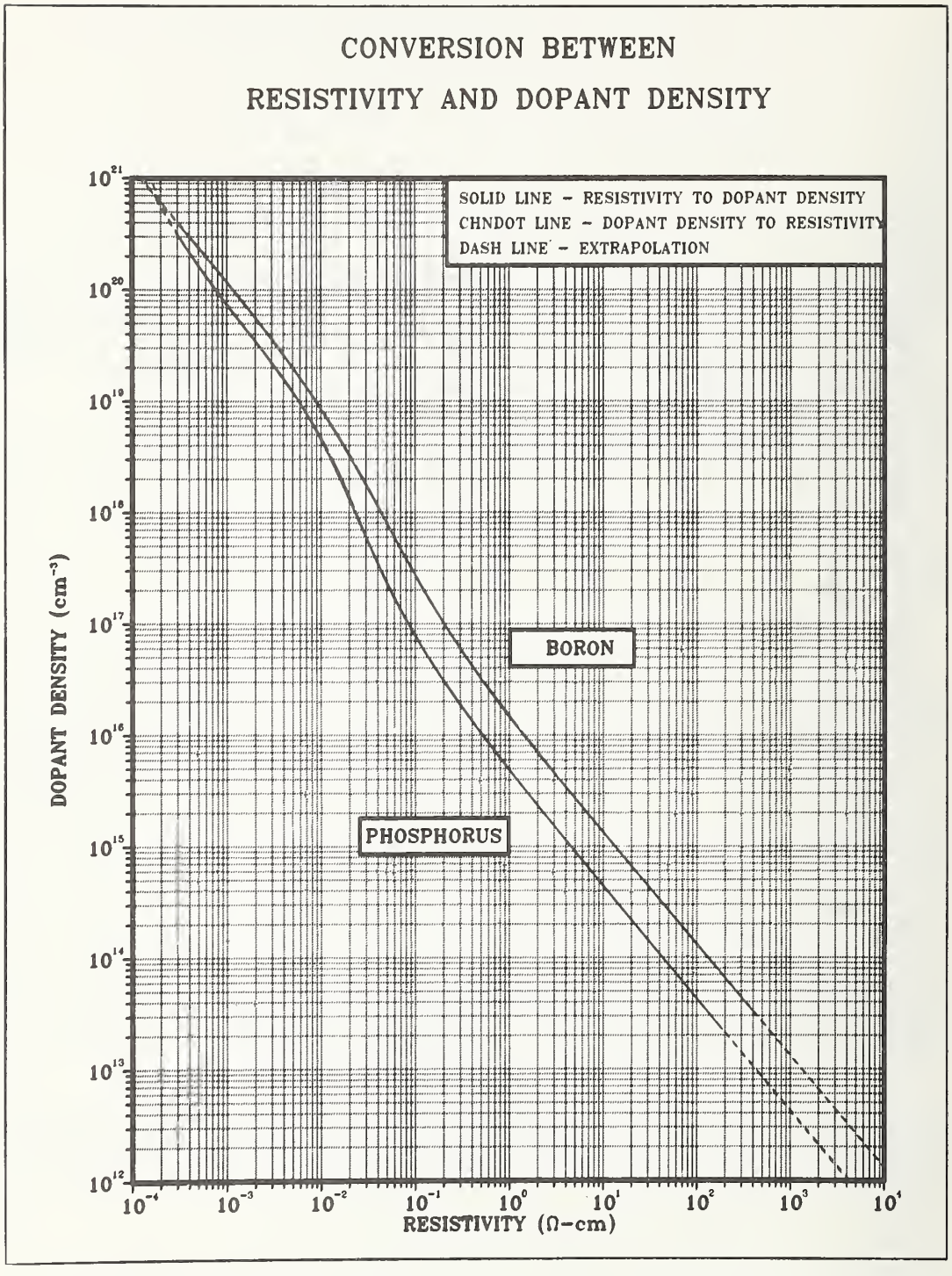

Figure 18. Dopant density *versus* resistivity at 23°C for silicon doped with phosphorus and with boron. The solid line shows the dopant density calculated from the equation of the product as a function of resistivity for the region of actual data. The chaindot line shows the resistivity calculated from the equation of the product as a function of dopant density for the region of actual data. Dashed lines show the extrapolation beyond the region covered by the data. On the scale of the figure shown here, the solid and chaindot lines are indistinguishable. However, in regions where the self-consistency error is appreciable, the lines are distinguishable on the wall chart available from ASTM. (Graph is from ASTM document F 723 cited in the text.)

Boron- and Phosphorus-Doped Silicon" which has been approved by Committee F-1 on Electronics and will appear in the 1981 Annual Book of ASTM Standards, Part 43. This document provides three procedures for converting between resistivity and dopant density at 23°C. They are: (1) graphical method - a graph, reproduced as figure 18 of this report, with curves for both boron and phosphorus; (2) tabular method - a set of four tables covering the two dopants as functions of both resistivity and dopant density; and (3) computational method - the same equations and coefficients as given in this report for use when exact calculations are most convenient or necessary. The document does not cover electron or hole mobility relationships.

9. CONCLUSIONS

For phosphorus-doped silicon, the relationship between resistivity and dopant density was determined for densities between 10^{13} and 10^{20} cm^{-3}. The results differ from the *n*-type Irvin curve by 5 to 15 percent, always in the direction of lower resistivity for a given dopant density. The work is in agreement with that of Mousty *et al.* in the 10^{15} to 10^{18} cm^{-3} range, but differences exist for lower and for higher doping levels.

For boron-doped silicon resistivity and dopant density data were obtained for boron densities between 10^{14} and 10^{20} cm^{-3}. The results differ significantly from the commonly used Irvin curve for densities greater than 10^{16} cm^{-3} with a maximum deviation of 45 percent at 5×10^{17} cm^{-3} in the direction of lower resistivity for a given boron density. Hole mobility values, calculated from this work with correction for percent ionization of the dopant atoms, are much larger than the experimental data of Tsao and Sah, but are in good agreement with the theoretical calculations of Li. The hole mobility values are in reasonable agreement with Wagner's work on boron-implanted silicon. The maximum discrepancy occurs in the 10^{18} cm^{-3} range where the Wagner mobility is 10 percent lower because deionization effects were not included.

Analytical expressions, convenient for engineering calculations, were fitted to the resistivity-dopant density data as a function of resistivity and dopant density for temperatures of both 23°C and 300 K. These fits are self-consistent within a few percent so that conversion can go both directions without iteration. Similar analytical expressions were fitted to the calculated hole mobility as a function of resistivity and hole density.

ACKNOWLEDGMENTS

The authors are indebted to D. R. Ricks for the mechanical four-probe resistivity measurements, to F. H. Brewer for the Hall effect measurements, and to J. Krawczyk and L. A. Robinson for specimen preparation. Special thanks are due M. G. Buehler for designing the test structures used in this work and R. D. Larrabee and W. M. Bullis for helpful comments on the manuscript. The typing of the report with its many tables was expertly done by Jane Walters and Jo Halapatz.

REFERENCES

1. Caughey, D. M., and Thomas, R. E., Carrier Mobilities in Silicon Empirically Related to Doping and Field, *Proc. IEEE* 55, 2192-2193 (1967).

2. Irvin, J. C., Resistivity of Bulk Silicon and of Diffused Layers in Silicon, *Bell System Tech. J.* 41, 387-410 (1962).

3. Baccarani, G., and Ostoja, P., Electron Mobility Empirically Related to the Phosphorus Concentration in Silicon, *Solid-State Electron.* 18, 579-580 (1975).

4. Wagner, S., Diffusion of Boron from Shallow Ion Implants in Silicon, *J. Electrochem. Soc.* 119, 1570-1576 (1972).

5. Thurber, W. R., Mattis, R. L., Liu, Y. M., and Filliben, J. J., Resistivity-Dopant Density Relationship for Phosphorus-Doped Silicon, *J. Electrochem. Soc.* 127, 1807-1812 (1980).

6. Thurber, W. R., Mattis, R. L., Liu, Y. M. and Filliben, J. J., Resistivity-Dopant Density Relationship for Boron-Doped Silicon, *J. Electrochem. Soc.* 127, 2291-2294 (1980).

7. Standard Test Method for Measuring Radial Resistivity Variation on Silicon Slices, ASTM Method F 81, *Annual Book of ASTM Standards,* Part 43 (November 1980).

8. Buehler, M. G., and Thurber, W. R., A Planar Four-Probe Test Structure; for Measuring Bulk Resistivity, *IEEE Trans. Electron Devices* ED-23, 968-974 (1976).

9. Test Method for Net Carrier Density in Silicon Epitaxial Layers by Voltage-Capacitance of Gated and Ungated Diodes, ASTM Method F 419, *Annual Book of ASTM Standards,* Part 43 (November 1980).

10. Buehler, M. G., *Semiconductor Measurement Technology:* Microelectronic Test Pattern NBS-3 for Evaluating the Resistivity-Dopant Density Relationship of Silicon, NBS Spec. Publ. 400-22 (June 1976).

11. Thurber, W. R., and Buehler, M. G., *Semiconductor Measurement Technology:* Microelectronic Test Pattern NBS-4, NBS Spec. Publ. 400-32 (April 1978).

12. Leedy, T. F., and Liu, Y. M., *Semiconductor Measurement Technology:* Microelectronic Processing Laboratory at NBS, NBS Spec. Publ. 400-53 (December 1978).

13. Standard Method for Measuring Resistivity of Silicon Slices with a Collinear Four-Probe Array, ASTM Method F 84, *Annual Book of ASTM Standards,* Part 43 (November 1980).

14. Grove, A. S., *Physics and Technology of Semiconductor Devices* (John Wiley and Sons, Inc., New York, 1967), pp. 278-285.

15. Gillilland, K. E., Cook, H. D., Mielenz, K. D., and Stephens, R. B., Use of a Laser for Length Measurement by Fringe Counting, *Metrologia* 2, 95-98 (1966).

16. McDonald, B., and Goetzberger, A., Measurement of the Depth of Diffused Layers in Silicon by the Grooving Method, *J. Electrochem. Soc.* 109, 141-144 (1962).

17. Mattis, R. L., and Buehler, M. G., *Semiconductor Measurement Technology:* A BASIC Program for Calculating Dopant Density Profiles from Capacitance-Voltage Data, NBS Spec. Publ. 400-11 (June 1975).

18. Mattis, R. L., and Buehler, M. G., A New Method for Calculating Background Dopant Density from *p-n* Junction Capacitance-Voltage Measurements, *J. Electrochem. Soc.* 124, 1918-1923 (1977).

19. Dunlap, W. C., Jr., and Watters, R. L., Direct Measurement of the Dielectric Constants of Silicon and Germanium, *Phys. Rev.* 92, 1396-1397 (1953).

20. Bullis, W. M., Brewer, F. H., Kolstad, C. D., and Swartzendruber, L. J., Temperature Coefficient of Resistivity of Silicon and Germanium Near Room Temperature, *Solid-State Electron.* 11, 639-646 (1968).

21. van der Pauw, L. J., A Method of Measuring Specific Resistivity and Hall Effect of Discs of Arbitrary Shape, *Philips Res. Rep.* 13, 1-9 (1958).

22. David, J. M., and Buehler, M. G., A Numerical Analysis of Various Cross Sheet Resistor Test Structures, *Solid-State Electron.* 20, 539-543 (1977).

23. Measuring Hall Mobility and Hall Coefficient in Extrinsic Semiconductor Single Crystals, ASTM Method F 76, *Annual Book of ASTM Standards,* Part 43 (November 1980).

24. Beer, A. C., Galvanomagnetic Effects in Semiconductors, *Solid State Phys.*, F. Seitz and D. Turnbull, Eds., Suppl. 4, pp. 99-266 (Academic Press, New York, 1963).

25. Morin, F. J., and Maita, J. P., Electrical Properties of Silicon Containing Arsenic and Boron, *Phys. Rev.* 96, 28-35 (1954).

26. Wolfstirn, K. B., Hole and Electron Mobilities in Doped Silicon from Radiochemical and Conductivity Measurements, *J. Phys. Chem. Solids* 16, 279-284 (1960).

27. Schroder, D. K., Braggins, T. T., and Hobgood, H. M., The Doping Concentrations of Indium-Doped Silicon Measured by Hall, C-V and Junction-Breakdown Techniques, *J. Appl. Phys.* 49, 5256-5259 (1978).

28. Linares, L. C., The Mobility, Resistivity and Carrier Density in *p*-Type Silicon Doped with Boron, Gallium and Indium, Ph.D. Dissertation, University of Florida, 1979.

29. Nakagawa, N., and Zukotynski, S., Drift Mobility and Hall Coefficient Factor of Holes in Germanium and Silicon, *Can. J. Phys.* 56, 364-372 (1978); and Lin, J. F., Li, S. S., Linares, L. C., and Teng, K. W., Theoretical Analysis of Hall Factor and Hall Mobility in p-Type Silicon (to be published in *Solid-State Electron.*, 1981).

30. Li, S. S., and Thurber, W. R., The Dopant Density and Temperature Dependence of Electron Mobility and Resistivity in *n*-Type Silicon, *Solid-State Electron.* 20, 609-616 (1977).

31. Thurber, W. R., Comparison of Measurement Techniques for Determining Phosphorus Densities in Semiconductor Silicon, *J. Electron. Materials* 9, 551-560 (1980).

32. Mousty, F., Ostoja, P., and Passari, L., Relationship Between Resistivity and Phosphorus Concentration in Silicon, *J. Appl. Phys.* 45, 4576-4580 (1974).

33. Fair, R. B., Analysis of Phosphorus-Diffused Layers in Silicon, *J. Electrochem. Soc.* 125, 323-327 (1978).

34. Plunkett, J. C., Stone, J. L., and Leu, A., A Computer Algorithm for Accurate and Repeatable Profile Analysis Using Anodization and Stripping of Silicon, *Solid-State Electron.* 20, 447-453 (1977).

35. Fair, R. B., and Tsai, J. C. C., A Quantitative Model for the Diffusion of Phosphorus in Silicon and the Emitter Dip Effect, *J. Electrochem. Soc.* 124, 1107-1118 (1977).

36. Masetti, G., and Solmi, S., Relationship between Carrier Mobility and Electron Concentration in Silicon Heavily Doped with Phosphorus, *Solid-State and Electron. Devices* 3, 65-68 (1979).

37. Li, S. S., The Dopant Density and Temperature Dependence of Hole Mobility and Resistivity in Boron Doped Silicon, *Solid-State Electron.* 21, 1109-1117 (1978). See also Li, S. S., *Semiconductor Measurement Technology:* The Theoretical and Experimental Study of the Temperature and Dopant Density Dependence of Hole Mobility, Effective Mass, and Resistivity in Boron-Doped Silicon, NBS Spec. Publ. 400-47 (November 1979); and Linares, L. C., and Li, S. S., An Improved Model for Analyzing Hole Mobility and Resistivity in *p*-Type Silicon Doped with Boron, Gallium, and Indium, *J. Electrochem. Soc.* 128, 601-608 (1981).

38. Thurber, W. R., and Carpenter, B. S., Boron Determination in Silicon by the Nuclear Track Technique, *J. Electrochem. Soc.* 125, 654-657 (1978).

39. Chapman, P. W., Tufte, O. N., Zook, J. D., and Long, D., Electrical Properties of Heavily Doped Silicon, *J. Appl. Phys.* 34, 3291-3295 (1963).

40. Crowder, B. L., The Influence of the Amorphous Phase on Ion Distributions and Annealing Behavior of Group III and Group V Ions Implanted into Silicon, *J. Electrochem. Soc.* 118, 943-952 (1971).

41. Tsao, K. Y., and Sah, C. T., Temperature Dependence of Resistivity and Hole Conductivity Mobility in *p*-Type Silicon, *Solid-State Electron.* 19, 949-953 (1976). See also Woodley, T. J., and Sah, C. T., Deionization Effect on the Evaluation of Hole Mobility in *p*-Si, *Solid-State Electron.* 20, 385-388 (1977).

42. Filliben, J. J., DATAPLOT - Command Manual: ... Fit, NBS Statistical Engineering Division Working Paper 80-1, 1980 (formal NBS publication to follow).

43. Esaki, L., and Miyahara, Y., A New Device Using the Tunneling Process in Narrow *p-n* Junctions, *Solid-State Electron.* 1, 13-21 (1960).

44. Omel'yanovskii, E. M., Fistul', V. I., and Mil'vidskii, M. G., Electron Mobility in Heavily Doped Silicon, *Sov. Phys. - Solid State* 5, 676-680 (1963).

45. Yamanouchi, C., Mizuguchi, K., and Sasaki, W., Electric Conduction in Phosphorus Doped Silicon at Low Temperatures, *Jap. J. Phys. Soc.* 22, 859-864 (1967).

46. Logan, R. A., Gilbert, J. F., and Trumbore, F. A., Electron Mobilities and Tunneling Currents in Silicon, *J. Appl. Phys.* 32, 131-132 (1961).

NBS-114A (REV. 2-8C)

U.S. DEPT. OF COMM. BIBLIOGRAPHIC DATA SHEET (See instructions)	1. PUBLICATION OR REPORT NO. NBS SP 400-64	2. Performing Organ. Report No.	3. Publication Date May 1981

4. TITLE AND SUBTITLE

Semiconductor Measurement Technology: The Relationship Between Resistivity and Dopant Density for Phosphorus- and Boron-Doped Silicon

5. AUTHOR(S)

W. R. Thurber, R. L. Mattis, Y. M. Liu, and J. J. Filliben

6. PERFORMING ORGANIZATION (If joint or other than NBS, see instructions)

NATIONAL BUREAU OF STANDARDS
DEPARTMENT OF COMMERCE
WASHINGTON, D.C. 20234

7. Contract/Grant No.
ARPA Order No. 2397
Program Code 7Y10

8. Type of Report & Period Covered
Final

9. SPONSORING ORGANIZATION NAME AND COMPLETE ADDRESS (Street, City, State, ZIP)

Defense Advanced Research Projects Agency
1400 Wilson Boulevard
Arlington, VA 22209

and

National Bureau of Standards
Washington, DC 20234

10. SUPPLEMENTARY NOTES

Library of Congress Catalog Card Number 81-600052.
Conducted as part of the NBS Semiconductor Technology Program.

☐ Document describes a computer program; SF-185, FIPS Software Summary, is attached.

11. ABSTRACT (A 200-word or less factual summary of most significant information. If document includes a significant bibliography or literature survey, mention it here)

New data have been obtained for the resistivity-dopant density relationship for silicon doped with phosphorus or boron for dopant densities in the range 10^{13} to 10^{20} cm^{-3}. For dopant densities less than 10^{18} cm^{-3}, results were calculated from resistivity and junction capacitance-voltage measurements on processed wafers. For more heavily doped material, data were obtained from Hall effect and resistivity measurements on specimens cut from bulk silicon slices. These primary methods were supplemented for phosphorus-doped material by neutron activation analysis and a photometric technique and for boron-doped material by the nuclear track technique. For phosphorus-doped silicon the results of this work differ by 5 to 15 percent from the commonly used Irvin curve, always in the direction of lower resistivity for a given dopant density. For boron-doped silicon the results differ significantly from the *p*-type Irvin curve for boron densities greater than 10^{16} cm^{-3} with a maximum deviation of 45 percent at 5×10^{17} cm^{-3} in the direction of lower resistivity for a given dopant density. Hole mobility values derived from the data are in reasonable agreement with the Wagner expression with a maximum discrepancy of 10 percent in the 10^{18} cm^{-3} range. Analytical curves were fitted to the resistivity-dopant density product as a function of resistivity and dopant density for temperatures of 23°C and 300 K. Similar curves were obtained for the calculated carrier mobility as a function of resistivity and carrier density.

12. KEY WORDS (Six to twelve entries; alphabetical order; capitalize only proper names; and separate key words by semicolons)

Boron; capacitance-voltage technique; dopant density; electron mobility; Hall effect; hole mobility; Irvin curves; phosphorus; resistivity; semiconductor; silicon.

13. AVAILABILITY

☒ Unlimited
☐ For Official Distribution. Do Not Release to NTIS
☒ Order From Superintendent of Documents, U.S. Government Printing Office, Washington, D.C. 20402.
☐ Order From National Technical Information Service (NTIS), Springfield, VA. 22161

14. NO. OF PRINTED PAGES
53

15. Price
$3.25

☆ U.S. GOVERNMENT PRINTING OFFICE : 1981 O—340-997 (1646)

USCOMM-DC 6043-P80

Announcement of Semiconductor Measurement Technology
List of Publications 72 – 1962-1980

Chief
Electron Devices Division
National Bureau of Standards
Bldg. 225, Room A305
Washington, DC 20234

Dear Sir:

Please send a copy of your latest "Semiconductor Measurement Technology, List of Publications 72."

Name _____

Company _____

Address _____

City _____ State _____ Zip Code _____

NBS TECHNICAL PUBLICATIONS

PERIODICALS

JOURNAL OF RESEARCH—The Journal of Research of the National Bureau of Standards reports NBS research and development in those disciplines of the physical and engineering sciences in which the Bureau is active. These include physics, chemistry, engineering, mathematics, and computer sciences. Papers cover a broad range of subjects, with major emphasis on measurement methodology and the basic technology underlying standardization. Also included from time to time are survey articles on topics closely related to the Bureau's technical and scientific programs. As a special service to subscribers each issue contains complete citations to all recent Bureau publications in both NBS and non-NBS media. Issued six times a year. Annual subscription: domestic $13; foreign $16.25. Single copy, $3 domestic; $3.75 foreign.

NOTE: The Journal was formerly published in two sections: Section A "Physics and Chemistry" and Section B "Mathematical Sciences."

DIMENSIONS/NBS—This monthly magazine is published to inform scientists, engineers, business and industry leaders, teachers, students, and consumers of the latest advances in science and technology, with primary emphasis on work at NBS. The magazine highlights and reviews such issues as energy research, fire protection, building technology, metric conversion, pollution abatement, health and safety, and consumer product performance. In addition, it reports the results of Bureau programs in measurement standards and techniques, properties of matter and materials, engineering standards and services, instrumentation, and automatic data processing. Annual subscription: domestic $11; foreign $13.75.

NONPERIODICALS

Monographs—Major contributions to the technical literature on various subjects related to the Bureau's scientific and technical activities.

Handbooks—Recommended codes of engineering and industrial practice (including safety codes) developed in cooperation with interested industries, professional organizations, and regulatory bodies.

Special Publications—Include proceedings of conferences sponsored by NBS, NBS annual reports, and other special publications appropriate to this grouping such as wall charts, pocket cards, and bibliographies.

Applied Mathematics Series—Mathematical tables, manuals, and studies of special interest to physicists, engineers, chemists, biologists, mathematicians, computer programmers, and others engaged in scientific and technical work.

National Standard Reference Data Series—Provides quantitative data on the physical and chemical properties of materials, compiled from the world's literature and critically evaluated. Developed under a worldwide program coordinated by NBS under the authority of the National Standard Data Act (Public Law 90-396).

NOTE: The principal publication outlet for the foregoing data is the Journal of Physical and Chemical Reference Data (JPCRD) published quarterly for NBS by the American Chemical Society (ACS) and the American Institute of Physics (AIP). Subscriptions, reprints, and supplements available from ACS, 1155 Sixteenth St., NW, Washington, DC 20056.

Building Science Series—Disseminates technical information developed at the Bureau on building materials, components, systems, and whole structures. The series presents research results, test methods, and performance criteria related to the structural and environmental functions and the durability and safety characteristics of building elements and systems.

Technical Notes—Studies or reports which are complete in themselves but restrictive in their treatment of a subject. Analogous to monographs but not so comprehensive in scope or definitive in treatment of the subject area. Often serve as a vehicle for final reports of work performed at NBS under the sponsorship of other government agencies.

Voluntary Product Standards—Developed under procedures published by the Department of Commerce in Part 10, Title 15, of the Code of Federal Regulations. The standards establish nationally recognized requirements for products, and provide all concerned interests with a basis for common understanding of the characteristics of the products. NBS administers this program as a supplement to the activities of the private sector standardizing organizations.

Consumer Information Series—Practical information, based on NBS research and experience, covering areas of interest to the consumer. Easily understandable language and illustrations provide useful background knowledge for shopping in today's technological marketplace.

Order the **above** *NBS publications from: Superintendent of Documents, Government Printing Office, Washington, DC 20402.*

Order the **following** *NBS publications—FIPS and NBSIR's—from the National Technical Information Services, Springfield, VA 22161.*

Federal Information Processing Standards Publications (FIPS PUB)—Publications in this series collectively constitute the Federal Information Processing Standards Register. The Register serves as the official source of information in the Federal Government regarding standards issued by NBS pursuant to the Federal Property and Administrative Services Act of 1949 as amended, Public Law 89-306 (79 Stat. 1127), and as implemented by Executive Order 11717 (38 FR 12315, dated May 11, 1973) and Part 6 of Title 15 CFR (Code of Federal Regulations).

NBS Interagency Reports (NBSIR)—A special series of interim or final reports on work performed by NBS for outside sponsors (both government and non-government). In general, initial distribution is handled by the sponsor; public distribution is by the National Technical Information Services, Springfield, VA 22161, in paper copy or microfiche form.

U.S. DEPARTMENT OF COMMERCE
National Bureau of Standards
Washington, D C 20234

OFFICIAL BUSINESS

Penalty for Private Use, $300

POSTAGE AND FEES PAID
U.S. DEPARTMENT OF COMMERCE
COM–215

U.S.MAIL

SPECIAL FOURTH-CLASS RATE
BOOK